Master of Science Thesis

Slow and Fast Hydrogen Deflagration
A validation study

Varun Jain

October 15, 2013

Faculty of Aerospace Engineering · Delft University of Technology

Slow and Fast Hydrogen Deflagration
A validation study

Master of Science Thesis

For obtaining the degree of Master of Science in Aerospace Engineering at Delft University of Technology

Varun Jain

October 15, 2013

Faculty of Aerospace Engineering · Delft University of Technology

Delft University Of Technology
Department Of
Aerodynamics

The undersigned hereby certify that they have read and recommend to the Faculty of Aerospace Engineering for acceptance of the thesis entitled **"Slow and Fast Hydrogen Deflagration"** by **Varun Jain** in partial fulfillment of the requirements for the degree of **Master of Science**.

Dated: October 15, 2013

Head of department: _____
Dr.ir. M.I. Gerritsma

Supervisor: _____
ir. Ed Komen

Reader: _____
Prof. dr. D.J.E.M. Roekaerts

Summary

Amidst the growing demand for energy, many nations are considering the expanded role of nuclear power in their energy portfolios. However, in case of severe accidents, large amounts of hydrogen gas can be released in the nuclear containment. Hydrogen-air mixture forms a very flammable gas which on subsequent ignition can lead to flame propagation in the nuclear containment. This may produce oscillating pressure waves or high over pressures that may damage the safety equipment and even affect the structural integrity of the nuclear reactor containment. Hence, there is a need for tools that can perform safety analysis of the nuclear reactors in case of severe accidents. In this respect, Computational Fluid Dynamics (CFD) codes have been widely used in the past to predict such flow and combustion phenomena. However, before any CFD code can be used for safety analysis, it requires thorough validation to corroborate the accuracy of its predicted results. This stems the motivation of the current thesis work.

In this thesis work we focus on the validation of the in-house CFD code developed by Nuclear Research and consultancy Group (NRG). Two different combustion models 1) the Zimont combustion model, and 2) the Lipatnikov combustion model are used for validation purpose. The validation study is performed in two different experiments 1) fast deflagration (high burning velocity of flame) ENACCEF RUN-153 experiment and, 2) slow deflagration (low burning velocity of flame) THAI HD-12 experiment. Furthermore, the importance of thermal radiation heat losses for flame propagation properties in both the experiments have been studied.

Both the combustion models are able to capture the physical phenomena observed in the experiments. However, it has been observed that the Zimont combustion model highly over predicts the flame velocity in slow deflagration regimes. The Lipatnikov combustion model predicts relatively lower flame velocity in the slow deflagration regime, giving a better agreement with the experimental results. Thus, the Lipatnikov combustion model can be seen as a melioration over the existing Zimont combustion model. Though, the author strongly suggests to perform more validation studies in different experimental conditions before this combustion model is used for further practical applications. Lastly, it has been shown that the thermal radiation heat losses do not affect the flame propagation properties significantly if the combustion times are too low. However, for longer flame

combustion times they tend to slow down the burning rate of the unburned gasses due to energy loss from the test facility in the form of thermal heat radiation.

With this work the author has made an attempt to create a base for further validation studies of Lipatnikov combustion model and hopes that this study will stimulate interest to further improve this combustion model.

Acknowledgements

It would be wrong to say that this work was a solitary effort and throughout theduration of my thesis I have received the help of many people.

First and foremost, my parents receive my deepest gratitude and love for their dedication and the many years of support that provided the foundation for this work.

I would like to express my gratitude to my advisor, Ed Komen, for his support, patience, and encouragement throughout my thesis work. It is not often that one finds an advisor and colleague that always finds the time for listening to the little problems and roadblocks that unavoidably crop up in the course of performing research. His technical and editorial advice was essential to the completion of this dissertation and has taught me innumerable lessons and insights on the workings of academic research in general.
My sincere regards are due to Dr. P. Sathiah for many valuable discussions on research in the field of combustion. And also for reviewing the previous drafts of this dissertation that further helped me to improve the presentation and contents of this dissertation. He has been a guiding spirit and inspired me to continue my education in the field of research.
I am thankful to Marc for guiding me guiding me with inputs throughout my thesis work.
My thanks also go to the members of the examination committee, Dr. Scarano and Dr. Roekaerts. I have taken exams with both of them and it has always been a learning experience in more than one ways.

The friendship of Abhineet, Darwin and Ram is much appreciated and has led to many interesting and good spirited discussions relating to this research and in general. I would be indebted for their support over the last two years. The MiniVan group for being there with me in the good & bad times and the interns at NRG/ECN for making my stay in Den Helder a memorable one. And a special mention of all of my office mates, Karolina, Valentina, Giulia, Iacopo, Tadej, and Tomasso. And the two people I have spent most of my time with, Giulia and Iacopo, working at NRG would not have been the same without you people (and the blame for delay in my graduation also goes to you!).

Finally, I would like to thank everyone who has helped me in one way or another.

Delft, The Netherlands Varun Jain
October 15, 2013

Contents

List of Figures

List of Tables

Nomenclature

Latin Symbols

$\dot{w}$	Rate of product creation	kg/m^3s
$\dot{w}_T$	Heat release due to combustion	J/m^3s
$\dot{w}_k$	Rate of creation of species k	kg/m^3s
BR	Blockage ratio	$n.a.$
c	Progress variable	$n.a.$
C_μ	Turbulence model constant	$n.a.$
C_D	Turbulent length scale constant	$n.a.$
C_p	Specific heat at constant pressure	kJ/kgK
$C_{\epsilon 1}$	Turbulunce model constant	$n.a.$
$C_{\epsilon 2}$	Turbulence model constant	$n.a.$
d_b	Baffle diameter	m
D_d	Diffusivity of deficient reactant	m^2/s
D_e	Diffusivity of excess reactant	m^2/s
D_k	Mass diffusivity of species k	m^2/s
d_p	Pipe diameter	m
Da	Damkohler number	$n.a.$
E	Total energy	J/kg
$f_{k,i}$	Volume force acting on species k in direction i	m/s^2
g_i	Component of gravitation vector in ith direction	m/s^2
h_k	Total enthalpy of species k	J/m^3
k	Turbulent kinetic energy	m^2/s^2

Ka	Karlovitz number	$n.a.$
l_t	Integral length scale	m
Le	Lewis number	$n.a.$
m	Total mass of the gas	kg
M_i	Molecular weight of species i	$kg/mole$
m_k	Mass of species k	kg
p	Pressure	Pa
P_b	Buoyancy term	kg/ms^3
P_k	Production term of turbulent kinetic energy	kg/ms^3
Pr	Prandtl Number	$n.a.$
Pr_t	Turbulent Prandtl number	$n.a.$
R	Universal gas constant	$J/moleK$
Re_t	Turbulent Reynolds number	$n.a.$
s_l	Laminar flame speed	m/s
Sc	Schmidt number	$n.a.$
T	Temperature	K
t	Time	s
u_i	Velocity in the i-direction	m/s
$V_{k,i}$	i component of the diffusion velocity of species k	m/s
x_i	Coordinate in the i-direction	m/s
Y_F	Fuel mass fraction	$n.a.$
Y_i	Mass fraction of species i	$n.a.$
Y_k	Mole fraction of species k	$n.a.$
Y_O	Oxidizer mass fraction	$n.a.$
$Y_{F,b}$	Burnt gas mass fraction	$n.a.$
$Y_{F,u}$	Unburned gas mass fraction	$n.a.$

Greek Symbols

α	Thermal diffusivity	m^2/s
β	Coefficient of thermal expansion	$1/K$
δ_l	Flame thickness	m
δ_{ij}	Kronecker symbol	$n.a.$
ϵ	Turbulent dissipation rate	m^2/s^3
λ	Thermal conductivity	W/mK
μ	Dynamic viscosity	m^2/s
ν	Kinematic viscosity	m^2/s
ϕ	Equivalence ratio	$n.a.$

ρ	Density	kg/m^3
σ_ϵ	Turbulence model constant	$n.a.$
σ_k	Turbulence model constan	$n.a.$
σ_{ij}	Sum of viscous and pressure tensor	N/m^2
τ_η	Kolmogorov time scale	m/s
τ_c	Chemical time scale	s
τ_t	Turbulent time scale	s
τ_{ij}	Viscous force tensor	N/m^2
u'	Turbulent r.m.s. velocity	m/s

Abbreviations

BR	Blockage Ratio
CFD	Computational Fluid Dynamics
CNRS	Centre National de la Recherche Scientifique
OECD	Organisation for Economic Co-operation and Development
PWR	Pressurized Water Reactor
TMI	Three Mile Island

Chapter 1

Introduction

1.1 Motivation

Today, many nations are considering an expanded role for nuclear power in their energy portfolios. This expansion is driven by concerns about global warming, growth in energy demand, and high costs of other alternative energy sources. In 2008, 435 nuclear reactors in 30 countries provided 16 % of the worlds electricity. In January 2009, 43 reactors were under construction in 11 countries, and several hundreds more were projected to come on-line globally by 2030. Among other factors such as nuclear waste disposal, impact on environment etc. nuclear saftey issues also pose a serious concern in the operation of nuclear reactors.

During a severe accident in a Pressurized Water Reactor (PWR), the reaction between steam and zirconium present in the fuel rods can generate large amounts of hydrogen [1]. The hydrogen-air mixture in the containment can form a very flammable gas mixture. Upon ignition the hydrogen-air mixture can result into the propagation of turbulent flames that can generate strong pressure waves that may possibly result in a shock wave. Such wave phenomena may damage the safety equipment inside the nuclear reactor and may even jeopardize the structural integrity of the nuclear containment. This is dangerous because nuclear containment is the last barrier between radioactive chemicals and the environment.

The potential danger of hydrogen combustion in nuclear reactors was first realized after the Three Mile Island (TMI) accident in March 1979, where the large quantity of hydrogen released in reactor containment led to subsequent burning. This resulted in an over pressure of 2 bars affecting the structural integrity of the nuclear reactor containment [2]. The Fukushima-Daiichi accident in March 2011 reasserted that the hydrogen combustion issue cannot be neglected and control of hydrogen risk is still a key safety issue for nuclear power plants [3]. Therefore, to ensure safe operation of nuclear reactors, it is necessary to develop methods and tools that can be used to evaluate the risks involved in case of such accidents in nuclear reactors. Performing experiments to understand the turbulent combustion phenomena can incur high costs and may not be always feasible. Therefore,

evaluation of such loads needs computational codes which can be used with a high level of confidence. In the past, Computational Fluid Dynamics (CFD) has proven to be an important and viable tool to predict flow and combustion phenomena. Hence, development of a modern CFD code for mechanistic description of hydrogen combustion in the reactor containment could be a viable route to evaluate the containment loads during hydrogen combustion.

1.2 Objectives

The main objective of this MSc thesis is to contribute to the development and validation of a combustion model for premixed hydrogen-air mixtures. More specifically, the objectives of the work performed in this MSc thesis are:

- To perform validation study in ENACCEF RUN-153 fast deflagration experiment using the Zimont combustion model [4] and the Lipatnikov combustion model [5];
- To perform validation study in THAI HD-12 slow deflagration experiment using the Zimont combustion model [4] and the Lipatnikov combustion model [5];
- To determine the effect of thermal radiation heat loss on the flame propagation properties.

1.3 Structure of thesis

A basic introduction to deflagration phenomena with details focussed on hydrogen-air mixtures is given in Chapter 2. Description of the experimetns chosen for validation purposes are given in Chapter 3. The governing equations and the details of the CFD modeling techniques are discussed in Chapter 4. The simulation results with the validation analyses are presented in Chapter 5. Conclusions and recommendations for future work are discussed in Chapter 6 and Chapter 7 respectively.

Chapter 2

Deflagration: An Introduction

Turbulent combustion is a complicated phenomenon involving a large number of physical and chemical time scales. Combustion alone, without turbulence, is an intrinsically complex process involving a large range of chemical time scales. Turbulent combustion resulting from two way interaction of chemistry and turbulence is a much more complicated phenomenon which is challenging the science community for the last few decades.

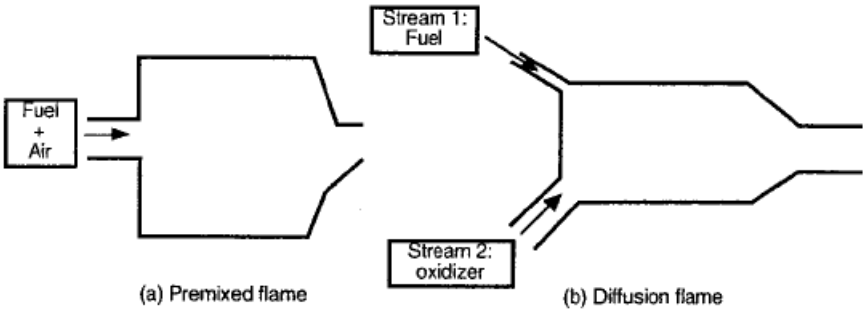

Figure 2.1: Premixed and non-premixed flame configurations. The figure has been taken from [6]

Basically, combustion can be divided into three sub-categories, premixed, non-premixed and partially premixed combustion. In premixed combustion, the fuel and oxidizer are mixed before they enter the combustion chamber [6] (see fig. 2.1a). In non-premixed combustion, also known as diffusion flames, the fuel and oxidizer are introduced separately into the combustion chamber through two (or more) inlets where flow rates and mass fractions are controlled separately (see fig. 2.1b). Partially premixed combustion is defined as a combustion process in which species are not perfectly mixed before combustion takes place but are better mixed than in a pure diffusion flame. Partially-premixed combustion can thus be interpreted as a combination of non premixed and premixed combustion. This thesis work is focused on premixed combustion of flames, and from here on we refer to premixed flames simply as flames, until and unless mentioned otherwise.

During premixed flame propagation, the speed at which the flame front travels relative to the unburned mixture is known as the flame speed. This speed may be affected by many parameters such as the concentration of the fuel in the mixture, the geometry of obstacles along path of the flame, dimensions of the enclosures, etc. Depending on flame speed, premixed flame can propagate in three modes:

- **Deflagration**: It is a process in which the flame front travels at subsonic speed relative to the unburned gas.
- **Deflagration to Detonation transition(DDT)**: During a deflagration wave propagation, a flame can accelerate under turbulent conditions and transform into a detonation wave. Turbulence enhances combustion to a point where a shock wave is formed just ahead of the flame front.
- **Detonation**: It is a process in which the flame front travels at a velocity greater than the speed of sound. The unburned mixture is heated by a shock wave behind which the mixture reaches a high temperature.

2.1 Laminar flames

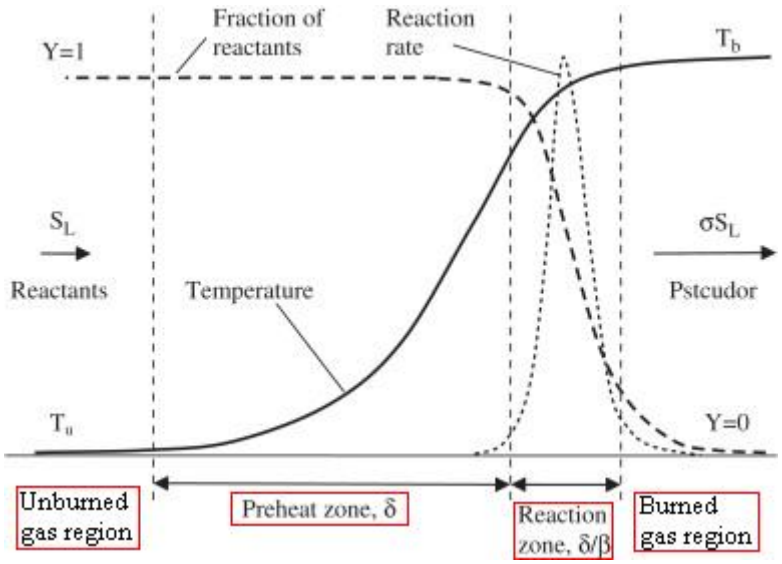

Figure 2.2: Laminar flame structure. The figure is taken from ref. [7]

The structure of a laminar flame consists of four distinct regions; 1) unburned region, 2) preheat region, 3) reaction zone, 4) burned gas region (see fig. 2.2). Initially, fresh unburned mixture at the ambient conditions is transported to the flame zone. As the mixture approaches the flame front, it is heated by conduction and radiation from the flame zone upstream. Chemical reaction and heat release are negligible at this stage. Once temperatures are hot enough to sustain combustion, chemical reaction takes place in the reaction zone. The gases emerging from this zone enter the burned gas zone where concentration and temperature are once again constant.

2.2 Laminar flame speed

The laminar flame speed is a fundamental property of laminar flames, such that at a given fuel-oxidizer concentration and initial value of pressure and temperature it always has the same value.

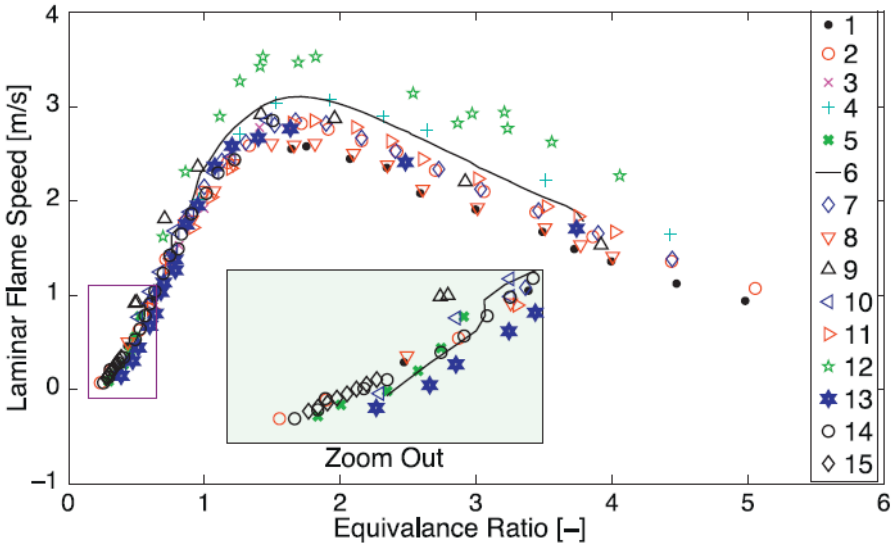

Figure 2.3: Laminar flame speed versus equivalence ratio for hydrogen-air mixtures at 100kPa and 298K. The symbols represent experimental data while solid line represents the simulations. The legend, referenced in [8], and are summarized as follows: 1) Aung et al. (1997) 2) Dowdy et al. (1993) 3) Wu and Law (1984) 4) Takahashi et al. (1983) 5) Vagelopoulos et al. (1994) 6) Conaire et al. (2004) 7) Taylor (1991) 8) Kwon and Faeth (2001) 9) Iijima and Takeno (1986) 10) Law (1993) 11) Tse et al. (2000) 12) Liu and MacFarlane (1983) 13)Lamoureux et al. (2003) 14) Egolfopoulos and Law (1991) and 15) Malet(2005) and Bleyer et al. (2012)

A wide spread in the values of laminar flame speeds of hydrogen air mixtures is observed in the combustion literature. Sathiah et al. [8] compared many correlations available in the combustion literature based on experimental results and numerical simulations. This comparison is shown in Fig. 2.3 with laminar flame speed from various research groups plotted as a function of the equivalence ratio ϕ.

Equivalence ratio of a given mixture is defined as the ratio of the fuel mass fraction to the oxidizer mass fraction in a mixture to that required for ideal stochiometric conditions. That is, it is given by,

$$\phi = \left(\frac{Y_F}{Y_O}\right) / \left(\frac{Y_F}{Y_O}\right)_{st}, \tag{2.1}$$

where Y_F is the fuel mass fraction, and Y_O is oxidizer mass fraction. For rich mixtures, the fuel is in excess, and $\phi > 1$. For lean mixture, the oxidizer is in excess, and $\phi < 1$.

In nuclear applications we generally deal with low equivalence ratio mixtures with $\phi = 0.2$ to 0.4. An enlarged zoom out of this area is also shown in Fig. 2.3. It can be observed that the spread in values of laminar flame speed is much less in this region. Therefore,

we have a conservative estimate of laminar flame speed for work performed in this thesis. However, for high equivalence ratios the laminar flame speed values are widely spread. Therefore, for applications that need laminar flame speed in this range, more experiments are required for its accurate estimation.

2.3 Turbulent flame speed

When flows entering a flame are turbulent, the laminar flame mode is replaced by a regime where turbulence and combustion interact. Unlike a laminar flame, where the flame speed depends on the thermal and chemical properties of the unburned mixture, the turbulent flame speed also depends on the behavior of the flow, as well as on the mixture properties. The effect of turbulence is to wrinkle and distort a laminar flame front. This flame front locally propagates with laminar flame speed s_l consistent with a plane laminar flame. For an observer traveling with the flame, a turbulent flame speed can be defined as the velocity at which reactants enter the flame zone in a direction normal to the flame. Since the direct measurement of unburned gas velocity at a point near a turbulent flame is exceedingly difficult, at best, flame velocities usually are determined from measurements of reactant mass flow rates. Thus, the turbulent flame speed is expressed as

$$\dot{m} = \rho_u \overline{A} s_t = \rho_u A_{fl} s_l \tag{2.2}$$

where, $\dot{m}$, is the mass flow rate of unburned gas, ρ_u is the unburned gas density, $\overline{A}$ is the time averaged mean flame surface area, s_t the turbulent flame speed, A_{fl} the instantaneous flame surface area and s_l the laminar flame speed.
Therefore, the ratio of the turbulent flame speed to the laminar flame sped is given by:

$$\frac{s_t}{s_l} = \frac{A_{fl}}{\overline{A}} \tag{2.3}$$

Before further discussion on turbulent flame speed, it is useful to define certain terms and non-dimensional numbers relevant for turbulent combustion.

Integral time scale: The integral length scale l_t is a physical quantity describing the size of the large energy containing eddies in a turbulent flow. The integral time scale is the time scale associated with these large eddies and is given by,

$$\tau_t = \frac{l_t}{u'} \text{ where } l_t = C_D \frac{(u')^3}{\epsilon}, \tag{2.4}$$

where u' is the r.m.s. of the turbulent velocity, $C_D = 0.37$ is the turbulent length scale constant, and ϵ is the turbulent dissipation rate.

Kolmogorov time scale: The time scale of the smallest eddies is associated with the Kolmogorov time scale which is defined as,

$$\tau_\eta = \left(\frac{\nu}{\epsilon}\right)^{1/2}, \tag{2.5}$$

where ν is the kinematic viscosity.

Chemical time scale: The chemical time scale, τ_c, is defined as,

$$\tau_c = \frac{\alpha}{s_l^2} \qquad \alpha = \frac{\lambda}{\rho C_p} \tag{2.6}$$

where α is the thermal diffusivity, s_l is laminar flame speed, λ is the thermal conductivity, ρ is the density, and C_p is the specific heat at constant pressure.

Flamelet: In premixed combustion flows, chemical activity often occurs in thin (in comparison with the integral length scale) and strongly wrinkled sheet like fronts [4]. These fronts are known as the flamelets.

Flame brush thickness: The flame brush thickness is a characteristic measure of the transition zone between the unburned and burned states of a premixed flame.

Damkohler number: The Damkohler number is defined as the ratio of the integral time scale to the chemical time scale, that is,

$$Da = \frac{\tau_t}{\tau_c}, \tag{2.7}$$

Small values of Da correspond to slow chemistry reactions and large values of Da corresponds to fast chemistry reactions.

Karlovitz number: It is defined as the ratio of the chemical time scale to the Kolmogorov time scale and is given by,

$$Ka = \frac{\tau_c}{\tau_\eta} = \frac{\delta^2}{\eta^2} = \frac{u_\eta^2}{s_l^2}, \tag{2.8}$$

where, δ is the flame brush thickness, η the length of smallest eddies in turbulence cascade, u_η is the velocity of the smallest eddies, and s_l the laminar flame speed. If $Ka \ll 1$, the chemical reactions occur much faster than all turbulent time scales. Turbulence does not alter the flame structure. As Ka is increased the flame is more prone to alterations by turbulent fluctuations.

Turbulent Reynolds number: The Reynolds number represents the ratio of the inertia forces to the viscous forces. It characterizes the extent of the turbulent energy cascade. The turbulent Reynolds number is based on the integral length scale of turbulence and the turbulence intensity and is given by,

$$Re_t = \frac{u' l_t}{\nu}, \tag{2.9}$$

Prandtl Number: The Prandtlt number is defined as the ratio of momentum diffusion and thermal diffusion and is given by,

$$Pr = \frac{\nu}{\alpha}, \tag{2.10}$$

Schmidt Number: The Schmidt number is defined as the ratio of momentum diffusion and mass diffusion and is given by,

$$Sc = \frac{\nu}{D}, \tag{2.11}$$

where, D is the mass diffusivity.

Lewis Number: The Lewis number is the ratio of thermal diffusion to mass diffusion given by,

$$Le = \frac{\alpha}{D} \tag{2.12}$$

2.4 Preferential Diffusion Thermal instability

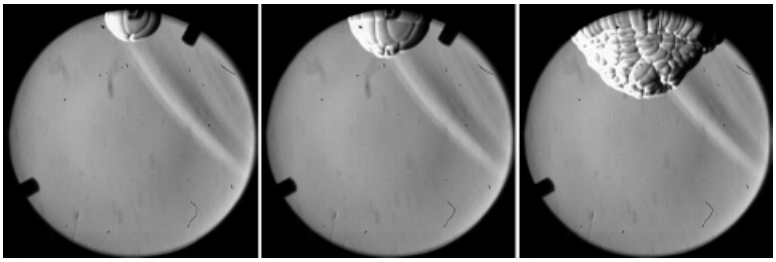

Figure 2.4: Evolution of Preferential Diffusion Thermal instability. Gradual growth and branching of large cracks on the flame surface indicates growth of PDT instability. The figure has been taken from [10].

The Preferential Diffusion Thermal (PDT) instability is a combination of diffusive and thermal instability. During flame propagation both mass and thermal diffusion exist across the flame surface [10]. At any instant, it is likely that molecular diffusion of the deficient reactant is larger than thermal diffusion, i.e. $D_d > \alpha$. In that case chemical energy supplied to the positively curved parts of the flame surface (upstream-pointing bulges) exceeds the heat losses due to molecular conductivity. Also, if the molecular diffusion of the deficient reactant is more than the molecular diffusion of the excess reactant, i.e. $D_d > D_e$, the mixture component in the bulges tend to stochiometric composition. Both these processes increase the flame speed locally in upstream pointing bulges. The opposite phenomenon occurs in downstream pointing bulges, i.e. the flame speed is decreased. This results in growing amplitude of flame front perturbations(bulges) [11]. In fig. 2.4, the evolution of unequal diffusion instability is shown. We can observe gradual growth and branching of large cracks in PDT instability. Very lean flames have a slow burning speed. Such slow burning speed gives cracks, which are formed due to initial spark defects or local heterogeneity or unequal diffusion effects, plenty of time to grow and branch. Thus, very lean flames are often born with large cracks due to the PDT instability.

Lean hydrogen-air mixtures have low Lewis numbers, i.e. $D_d > \alpha$, and therefore, high thermal instability. Thus it is important to take into account the PDT instability effects when considering lean hydrogen air mixtures, or in general mixtures with low Lewis numbers.

2.5 Turbulent premixed flames

Due to the presence of initial turbulence levels and combustion instabilities (discussed in previous section), the laminar premixed flame can transform into a turbulent premixed flame. The governing physical mechanism of premixed turbulent flame propagation are commonly described using the Borghi diagram (see fig. 2.5) which is discussed in the next paragraphs.

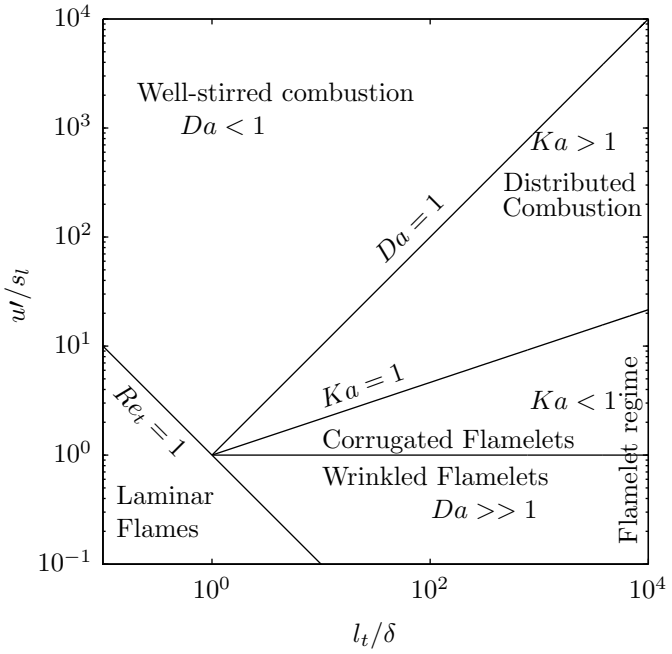

Figure 2.5: The Borghi Diagram. The figure has been extracted from [5]

In the Borghi diagram Fig. 2.5, the lines $Re_t = 1$, $Da = 1$, and $Ka = 1$ represent the boundaries between the different regimes of premixed turbulent combustion. Another boundary of interest is $u' = s_l$ whcih separates the wrinkled flamelets from the corrugated flamelets. These regimes are explained below [12].

- **Laminar flames**: The line $Re_t = 1$ separates the laminar flames $Re_t < 1$ form the turbulent flames $Re_t > 1$.
- **Wrinkled flamelets**: In this regime $u' < s_l$, i.e., even the large eddies cannot convolute the the flame front. Therefore, the flame displacement by s_l is faster than the displacement by turbulence with u' in this regime. That is flame propagation is dominating than the turbulence. The flamelet structure remains close to that of laminar flames.
- **Corrugated flamelets**: In this regime we have $Ka < 1$ and $u' > s_l$. Therefore, using Eq. 2.8,

$$u' \geq s_l \geq u_\eta \tag{2.13}$$

The velocity of larger eddies is larger than the burning velocity, thus, these eddies will push the flame front around causing convolution of the flame surface. The smallest eddies have a velocity less than the burning velocity, and will not wrinkle the flame front. Therefore, the larger eddies interact with the flame and unburned pockets are formed that penetrate inside the flame brush and are eventually consumed by the flame advancement. At sufficiently low turbulence levels, the mean thickness of a turbulent flame should be increased by this mechanism.

- **Distributed combustion**: In this regime, $Ka < 1$, i.e. $\eta < \delta$ (using Eq. 2.8). Therefore , even the smallest eddies can enter into the flamelet structure. Thus, the flame is thickened by turbulent eddies. This results in intensified heat and mass transfer across the flame. This regime is also known as thickened flame regime or distributed reaction zone.

- **Well-stirred combustion**: In this regime, $Da < 1$, i.e. the chemistry is slow. Turbulence homogenizes the flow field by rapid mixing, leaving the slow chemistry to be the rate determining process. No specific interaction between turbulence and combustion can occur in this regime.

Chapter 3

Selected facilities and experiments for validation

3.1 ENACCEF facility

The experiments were conducted in the ENACCEF test facility located in Orléans, France. The measurements were performed by Centre National de la Recherche Scientifique [13]. The test facility consists of a dome and acceleration tube, as shown fig. 3.1. The acceleration tube is 3.2 m long and has an internal diameter of 0.154 m with a total volume of 62.1 l. It consist of 9 annular baffles with varying blockage ratio. The blockage ratio is defined as:

$$BR = [1 - (\frac{d_b}{d_p})^2], \tag{3.1}$$

Here, d_b and d_p are the baffle and the pipe diameter, respectively.
The first baffle is located at a distance of 0.776 m and the distance between subsequent baffles is 0.154 m. The thickness of the baffles is 2 mm. The dome is 1.7 m long and has an internal diameter of 0.738 m with a volume of 658 l. The ENACCEF experiments were

Table 3.1: Experiments performed in ENACCEF facility

Experiment	Hydrogen concentration	Blockage Ratio	Mixture %
765	11.6-8.1	0.63	Negative gradient
736	11.4-5.8	0.63	Negative gradient
733	5.7-12	0.63	Positive gradient
160	13	0	Uniform
158	13	0.33	Uniform
153	13	0.63	Uniform

performed in 2010. Several hydrogen-air flame propagation experiments were performed

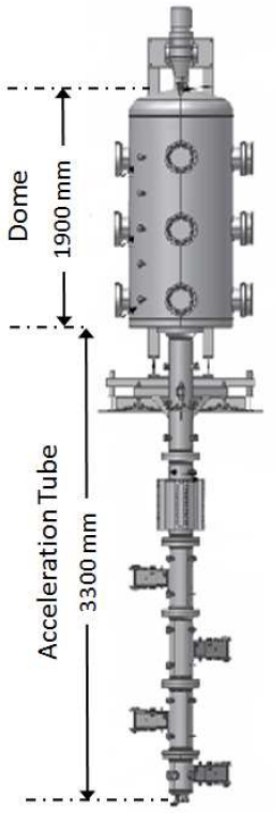

Figure 3.1: The ENACCEF facility. The figure has been taken from ref. [13]

out of which six experiments were used for code benchmarking within an European and International OECD project. Three tests (RUN 765, 736 and 733) with non-uniform mixtures, and three tests with uniform mixtures were used for CFD code benchmarking. These experiments are summarized in Table 3.1. The objective of the tests with non-uniform mixtures was to investigate the effects of hydrogen concentration gradients on flame propagation and pressure dynamics. The objective of the tests with uniform concentration with different blockage ratios was to investigate the effect of blockage ratio on flame propagation and pressure dynamics.

In this thesis work, we have used the ENACCEF RUN 153 experiment which has the uniform concentration of hydrogen gas of 13% by vol., with a blockage ratio BR of 0.63. In this experiment, the flame and pressure dynamics at an initial temperature of 296 K and a pressure of 100 kPa are investigated. The mixture is ignited using two thin tungsten electrodes (2 mm in diameter) which are linked to a high voltage source (10 kV). The voltage and intensity of the discharge are adjustable. The spark energy delivered is estimated to be between 10 and 20 mJ. The ignition point is located 0.138 m from the bottom of the facility.

To measure **flame position**, 16 UV-sensitive photomultiplier tubes (PMT) were used. The sensors were located at the following axial locations x = [0.277, 0.527, 0.777, 1.027, 1.277, 1.527, 1.772, 2.037, 2.377, 2.627, 2.877, 3.3415, 3.5915, 3.8415, 4.0915, 4.3415] m. The distances specified above are measured from the ignition point. The presence of the

flame was detected based on the total emission of the flame recorded using PMT. Using this method, OH radical is measured because of its high concentration in the flame front and in the burnt gases. The uncertainty in the flame position measurement is 8 mm.

The **pressure signal** was measured using high speed pressure transducers (7 Chimie Metal and 2 Kistler) which are mounted in the inner surface of the tube. The pressure transducers are located at the following axial locations x = [0.527, 1.027, 1.527, 2.139, 2.377, 2.627, 4.779] m and x = [2.877, 4.879] m.

It is worth stressing here, that in these experiments, the initial turbulence levels and the heat losses from the test facility were not measured.

3.2 THAI facility

The THAI-HD (HD=Hydrogen Deflagration) tests were performed in the THAI containment test facility which is operated by Becker Technologies GmbH at Eschborn, Germany, under the sponsorship of the German Federal Ministry of Economics and Technology [14].

The main component of the facility is a cylindrical stainless steel vessel of 9.2 m height and 3.2 m diameter with a total volume of 60 m^3. Its maximum allowable overpressure amounts to 14 bar at 180 °C.

Ignition process: Two spark igniters are used to begin the deflagration process. One spark igniter is located near the vessel bottom and one near the vessel top. For the HD-12 experiment bottom ignition was used to initiate upward deflagration.

Flame temperature and position detection: 43 fast sheathed thermocouples (outer diameter 0.25 mm) are installed at 13 different elevations, x = [0.7, 1.4, 2.1, 2.8, 3.5, 4.2, 4.9, 5.6, 6.3, 7.0, 7.7, 8.4, 9.1] m, in the test vessel to monitor the flame propagation (flame front arrival) and the flame temperature during hydrogen combustion. The location of flame position is determined when there is a sudden rise in the temperature of the sensor, and the corresponding time is recorded.

Pressure measurement: The initial vessel pressure is measured by one absolute-pressure transducer and two high precision manometers. The transient deflagration pressure is monitored by four fast pressure transducers (strain gauge type).

For the HD deflagration tests the THAI data acquisition system has been supplemented by additional data processing modules which permit to store the data of 48 fast channels with a sampling rate of 1 per millisecond (1000 Hz).

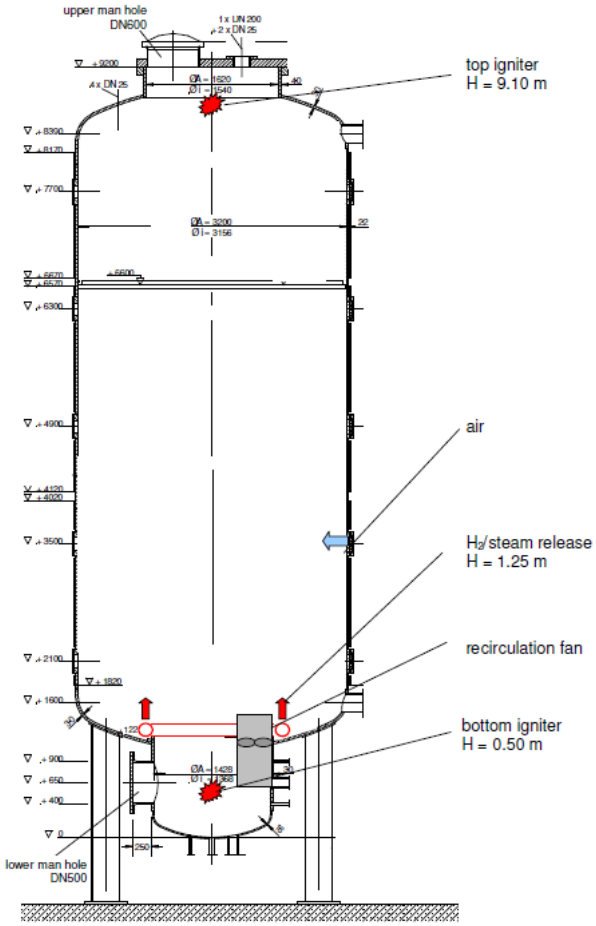

Figure 3.2: The THAI facility. The figure has been taken from ref. [14]

Chapter 4

CFD Modelling

Experimental studies of explosions are fundamental and essential to assess the risk from hydrogen-air explosions. Nonetheless, experiments alone cannot cover all scenarios and furthermore they offer an expensive solution. In this regard, CFD has been proven to be a useful tool to predict combustion flows using numerical techniques. Turbulent flows are encountered in most practical combustion systems and thus represent important phenomena when modelling combustion problems as well. Turbulent flows are difficult to compute because they are irregular and fluctuating; and most of the flow features occur at very small length and time scales. Resolving all these scales for practical applications is mostly not feasible due to the high computational costs involved. Therefore, the effect of turbulence has to be modelled for highly turbulent flows. Numerical solution of turbulent premixed combustion with CFD can be achieved by the following methods:

- **Reynolds Averaged Navier Stokes (RANS)**: This approach solves governing equations in ensemble averaged form. All scales of turbulence are modelled. The averaged equations need a closure model, that is, a turbulence model to close the Reynolds stress terms and a turbulent combustion model to close the turbulent reaction rate. The main advantage of RANS is that it is computationally cheap.

- **Unsteady-RANS(URANS)**: The URANS equations are the usual RANS equations, but with the transient (unsteady) term retained. This thesis work uses the URANS approach for obtaining numerical solutions. The main assumption in URANS is that the averaging time is higher than the Kolmogorov time scale, but much lower than the integral time scale. Hence, URANS can be used to capture low frequency phenomenon in a physical process.

- **Large Eddy Simulation(LES)**: In this method, the large scales of turbulence, or large eddies, are resolved on the numerical grid and smaller scales are modelled using a sub-grid scale model. Thus, the effect of modelling is reduced. The balance equations for LES are obtained by filtering the instantaneous balance equations. LES is computationally more expensive.

- **Hybrid RANS/LES**: The main bottle neck when using the LES approach is the requirement of very fine meshes near walls. Hybrid LES/RANS was invented to get rid of this limitation. In this method, unsteady RANS (URANS) is used near walls and away from walls LES is used.
- **Direct Numerical Simulation (DNS)**: In this approach the full instantaneous Navier-Stokes equations are solved at all length and time scales. DNS is computationally very expensive and therefore is used only for small scale combustion problems at low Reynolds numbers.

To enable the use of CFD as a predictive tool for consistent explosion risk assessment, it is essential that the model is validated against a large database of experiments. Once validated, a CFD tool will allow an outlining of the initial basis for guidance on risk reduction measures. This will be achieved by using CFD both to assist in the design of safer environments, and to address innovative safety concepts for nuclear containments [15].

4.1 Governing Equations

Turbulent combustion is a reacting flow process involving both fluid flow, heat transfer and chemistry. Therefore, together with the mass, momentum and energy conservation equations, additional species conservation equations are solved for all the species taking part in the reaction. The instantaneous governing equations for such flows are given as [6]:

Mass conservation

$$\frac{\partial \rho}{\partial t} + \frac{\partial}{\partial x_i}(\rho u_i) = 0, \tag{4.1}$$

where ρ is the density, t is the time, u_i the velocity components, and x_i the spatial coordinates.

Momentum conservation

$$\frac{\partial \rho u_j}{\partial t} + \frac{\partial}{\partial x_i}(\rho u_i u_j) = -\frac{\partial p}{\partial x_j} + \frac{\partial \tau_{ij}}{\partial x_i}, \tag{4.2}$$

where, p is the pressure, and τ_{ij} is the viscous stress tensor given by:

$$\tau_{ij} = \mu s_{ij} - \frac{2}{3}\mu \frac{\partial u_k}{\partial x_k}\delta_{ij}, \tag{4.3}$$

$$s_{ij} = (\frac{\partial u_j}{\partial x_j} + \frac{\partial u_j}{\partial x_i}), \tag{4.4}$$

where, μ is the dynamic viscosity and δ_{ij} is the Kronecker symbol.

Species conservation

$$\frac{\partial (\rho Y_k)}{\partial t} + \frac{\partial}{\partial x_i}(\rho u_i Y_k) = \frac{\partial}{\partial x_i}(D_k \rho \frac{\partial Y_k}{\partial x_i}) + \dot{w}_k \text{ for } k = 1, N, \tag{4.5}$$

where, D_k is mass diffusivity of species k, $\dot{w}_k$ is rate of creation of species k, and Y_k is the mass fraction of species k. The mass fraction of species is given by:

$$Y_k = \frac{m_k}{m}, \tag{4.6}$$

where, m_k is mass of the species k and m is the total mass of gas in volume.
In turbulent premixed combustion, it is a common practice to assume single one step chemistry of the form,

$$Fuel \longrightarrow Products, \tag{4.7}$$

in which we do not consider any intermediate radicals, and characterize the combustion process by a progress variable, c, defined as:

$$c = \frac{Y_F - Y_{F,u}}{Y_{F,b} - Y_{F,u}}, \tag{4.8}$$

where, $Y_{F,u}$ is fuel mass fraction in unburned gas and $Y_{F,b}$ is the fuel mass fraction in burned gas. Therefore, $c = 0$ in the unburned gas and $c = 1$ in the burned product gas [5].

Using this assumption and Eq. 4.8 we can simplify Eq. 4.5 as:

$$\frac{\partial(\rho c)}{\partial t} + \frac{\partial}{\partial x_i}(\rho u_i c) = \frac{\partial}{\partial x_i}(D\rho\frac{\partial c}{\partial x_i}) + \dot{w} \tag{4.9}$$

where D is the mass diffusivity of the unburned products and $\dot{w}$ the rate of product creation. The first term on RHS represents the diffusion flux of unburned species.

Energy conservation

$$\begin{aligned}\frac{\partial \rho E}{\partial t} + \frac{\partial}{\partial x_i}(\rho u_i E) &= \dot{w}_T + \frac{\partial}{\partial x_i}(\lambda\frac{\partial T}{\partial x_i} - \sum_{k=1}^{n} h_k Y_k V_{k,i}) \\ &\quad + \frac{\partial}{\partial x_j}(\sigma_{i,j}u_i) + \rho\sum_{k=1}^{n} Y_k f_{k,i}(u_i + V_{k,i}),\end{aligned} \tag{4.10}$$

where E is the total energy, $\dot{w}_T$ is the heat release due to combustion, λ is the thermal conductivity, h_k is the enthalpy of species k, $\sigma_{i,j}$ is the sum of viscous and pressure tensor, and $f_{k,j}$ is the volume force acting on species k. In the above Eq. 4.10 the second term on the RHS is the sum of heat diffusion flux and species diffusion flux, the third term denotes the viscous heating term and the last term is the power produced by volume forces f_k on species k.

Ideal gas law
The ideal gas law is used to calculate the density ρ as,

$$\rho = p/(RT\Sigma_{i=1}^{N}\frac{Y_i}{M_i}), \tag{4.11}$$

where p is the pressure, T is the temperature, N is the number of species, Y_i the mass fraction and M_i the molecular weight of species i.
In combustion flows, due to heat release we have variable density flows. If we use the

Reynolds averaging approach for turbulence modelling, we get unknown terms with density fluctuations. As an alternative approach, we use the Favre averaging approach, where any property f is expressed as density weighted mean averages by:

$$\tilde{f} = \frac{\overline{\rho f}}{\overline{\rho}} \tag{4.12}$$

Therefore, now, the quantity may be split in mean and fluctuating parts as:

$$f = \tilde{f} + f'' \quad \text{with} \quad \overline{\rho f''} = 0 \tag{4.13}$$

Thus, the governing Eq. 4.1 to 4.10 are now transformed to:

$$\frac{\partial \overline{\rho}}{\partial t} + \frac{\partial}{\partial x_i}(\overline{\rho}\tilde{u}_i) = 0 \tag{4.14}$$

$$\frac{\partial \overline{\rho}\tilde{u}_j}{\partial t} + \frac{\partial}{\partial x_i}(\overline{\rho}\tilde{u}_i\tilde{u}_j) + \frac{\partial \overline{p}}{\partial x_j} = \frac{\partial}{\partial x_i}(\overline{\tau}_{ij} - \overline{\rho}\widetilde{u_i'' u_j''}) \tag{4.15}$$

$$\frac{\partial(\overline{\rho}\tilde{c})}{\partial t} + \frac{\partial}{\partial x_i}(\overline{\rho}\tilde{u}_i\tilde{c}) = \frac{\partial}{\partial x_i}(\overline{\rho}D\frac{\partial \tilde{c}}{\partial x_i}) + \overline{\dot{w}} \tag{4.16}$$

$$\begin{aligned}\frac{\partial \overline{\rho}\tilde{E}}{\partial t} + \frac{\partial}{\partial x_i}(\overline{\rho}\tilde{u}_i\tilde{E}) = {} & \overline{\dot{w}}_T + \frac{\partial}{\partial x_i}(\overline{\lambda\frac{\partial T}{\partial x_i}} - \overline{\rho u_i'' h_s''}) + \overline{\tau_{ij}\frac{\partial u_i}{\partial x_j}} \\ & - \frac{\partial}{\partial x_i}(\overline{\rho\sum_{k=1}^{N} V_{k,i}Y_k h_{s,k}})\end{aligned} \tag{4.17}$$

4.2 Turbulence model

The Reynolds stress terms are modelled using the standard turbulence $k-\epsilon$ model. Using the Boussinesq hypothesis [6], the turbulent Reynolds stresses can be written as:

$$\overline{\rho u_i'' u_j''} = \overline{\rho}\widetilde{u_i'' u_j''} = -\mu_t(\frac{\partial \tilde{u}_i}{\partial x_j} + \frac{\partial \tilde{u}_j}{\partial x_i} - \frac{2}{3}\delta_{ij}\frac{\partial \tilde{u}_k}{\partial x_k}) + \frac{2}{3}\overline{\rho}k \tag{4.18}$$

where μ_t is turbulent dynamic viscosity, and $\delta_{i,j}$ is Kronecker symbol and k the turbulent kinetic energy, defined as:

$$k = \frac{1}{2}\sum_{k=1}^{3}\widetilde{u_k'' u_k''} \tag{4.19}$$

Using the standard $k-\epsilon$ model, the turbulent viscosity is approximated as:

$$\mu_t = \overline{\rho}C_\mu\frac{k^2}{\epsilon} \tag{4.20}$$

and k and ϵ are calculated from the following two closed eqns.:

$$\frac{\partial}{\partial t}(\overline{\rho}k) + \frac{\partial}{\partial x_i}(\overline{\rho}\tilde{u}_i k) = \frac{\partial}{\partial x_i}[(\mu + \frac{\mu_t}{\sigma_k})\frac{\partial k}{\partial x_i}] + P_k + P_b - \overline{\rho}\epsilon \tag{4.21}$$

$$\frac{\partial}{\partial t}(\overline{\rho}\epsilon) + \frac{\partial}{\partial x_i}(\overline{\rho}\tilde{u}_i \epsilon) = \frac{\partial}{\partial x_i}[(\mu + \frac{\mu_t}{\sigma_\epsilon})\frac{\partial \epsilon}{\partial x_i}] + C_{\epsilon 1}\frac{\epsilon}{k}P_k - C_{\epsilon 2}\overline{\rho}\frac{\epsilon^2}{k} \tag{4.22}$$

here the production term of turbulent kinetic energy P_k is given by,

$$P_k = -\overline{\rho}\widetilde{u_i''u_j''}\frac{\partial \tilde{u}_i}{\partial x_j}, \tag{4.23}$$

and the bouancy term P_b is given by,

$$P_b = \beta g_i \frac{\mu_t}{Pr_t}\frac{\partial \overline{T}}{\partial x_i}, \tag{4.24}$$

where Pr_t is the turbulent Prandtl number, g_i is the component of gravitational vector in ith direction, and β the coefficient of thermal expansion.

4.3 Combustion model

The central problem of numerical modelling of turbulent combustion consists of closing the source term $\overline{\dot{w}}$ in Eq. 4.16. Numerous models have been proposed by different research groups based on different approaches. A description of the most popular models is presented below:

Arrhenius Rate

The simplest approach for a combustion model is to assume that only chemistry plays an important role in determining the reaction rate. The Arrhenius equation gives the dependence of the rate constant k_r of chemical reactions on the temperature T and activation energy E_a. The rate of reaction is given by [16]

$$\overline{\rho}\tilde{\dot{w}} = A_f\overline{\rho}(1-\tilde{c})exp(-\frac{E_a}{R\tilde{T}}) \tag{4.25}$$

here, E_a is the activation energy and A_f is the pre-exponential factor.
This approach completely neglects the effect of turbulence and assumes that only chemistry plays an important role. This model becomes inaccurate due to the non-linear dependence of the rate of reaction on temperature and the large fluctuations of temperature in turbulent flames.

Eddy Break-up Model(EBU)

This model is based on phenomenological analysis of turbulent combustion for high turbulent Reynolds ($Re >> 1$) number & high Damkohler number ($Da >> 1$). The chemical kinetic rates are neglected and the mean reaction rate is mainly controlled by turbulent mixing time τ_t, given by [17]:

$$\overline{\rho}\tilde{\dot{w}} = -C_{EBU}\overline{\rho}\frac{\sqrt{\tilde{c''^2}}}{\tau_t} \tag{4.26}$$

$$\tag{4.27}$$

where $\tau_t = k/\epsilon$ is the turbulent time scale, C_{EBU} is a model constant, and $\tilde{c''^2}$ is the progress variable fluctuation. The square root is used for purely dimensional reason. For practical simulation purposes, $\tilde{c''^2}$ is modelled as:

$$\tilde{c''^2} = \tilde{c}(1-\tilde{c}) \tag{4.28}$$

Thus, the rate of reaction is given by:

$$\overline{\rho}\tilde{\dot{w}} = -\overline{\rho}C_{EBU}\frac{\epsilon}{k}\tilde{c}(1-\tilde{c}) \tag{4.29}$$

Eddy Dissipation Concept

The EDC model is based on the assumption that combustion occurs at the small scales, where mixing occurs on a molecular level and the rate is assumed to be proportional to the inverse of the turbulence time scale. It was developed from the original eddy break-up model, the most significant difference being that the EDC model accounts for the fact that reaction cannot occur unless both fuel and oxidizer mix on a molecular scale at a sufficiently high temperature. This is accomplished by relating the reaction rate to the limiting species. The model is formulated as [18]:

$$\overline{\rho}\tilde{\dot{w}} = B_1\overline{\rho}\frac{\epsilon}{k}min\left(\tilde{Y_F}, \frac{\tilde{Y_O}}{\phi}, B_2\frac{\tilde{Y_P}}{1+\phi}\right) \tag{4.30}$$

B1 and B2 are model constants, Y_F is the fuel mass fraction, Y_O is the oxidizer mass fraction, Y_P is the mass fraction of products, and ϕ is the equivalence ratio.

Zimont combustion model

The Zimont combustion model model assumes an increasing flame brush thickness according to the turbulent diffusion law. These flames with increasing flame brush thickness and constant combustion velocity are called intermediate steady propagation(ISP) flames. It is valid for $Re_t >> 1$, $Da >> 1$ and $u'_t >> s_f$ where s_f is the flamelet velocity. The reaction rate with this model is given as [4]:

$$\overline{\rho}\tilde{\dot{w}} = \rho_u s_t|\nabla c| \tag{4.31}$$

A sub-model for the turbulent flame speed, s_t, as a function of the physio-chemical properties of the combustible mixture and turbulence parameters is given as:

$$s_t = Au'_tDa^{1/4} = A(u')^{3/4}s_l^{1/2}\alpha^{-1/4}l_t^{1/4}, \tag{4.32}$$

where A is a model constant. In order to close Eq. 4.17, the mean heat release rate is obtained by multiplying the mean reaction rate $\dot{w}$ by the heat of combustion, ΔH of the fuel.

$$\tilde{\dot{w}_T} = \rho_u s_t|\nabla c|\Delta H \tag{4.33}$$

Lipatnikov combustion model

Lipatnikov [5] remarked on some of the drawbacks of the Zimont combustion model. These have been mentioned below:

- The sub-model Zimont combustion model uses for turbulent flame speed gives zero value for zero turbulence levels. However, at zero turbulence levels the turbulent flame speed should be equal to laminar flame speed s_L and not zero.

- The Zimont combustion model evaluates flame propagation of completely developed turbulent flames. It does not account for ignition modelling and laminar flame propagation and transition from laminar flames to turbulent flames.
- It cannot describe asymptotically completely developed turbulent flames characterized by steady mean flame brush thickness.

Lipatnikov [5] addresses some of these limitations, by extending and modifying the Zimont combustion model. He proposed an additional transient source term given by:

$$\overline{\rho}\tilde{\dot{w}}_2 = \frac{s_l^2}{4(\overline{D} + D_{t,t})}\rho_u \tilde{c}(1-\tilde{c}), \tag{4.34}$$

where $\overline{D}$ is the laminar diffusive term and $D_{t,t}$ is the time turbulent diffusive term given by,

$$D_{t,t} = D_t[1 - exp(-\frac{t_{fd}}{\tau'}], \tag{4.35}$$

where t_{fd} is the flame development time $t_{fd} = t - t_i$, t_i is the time at which the flame is ignited.
The complete source term is now given by,

$$\overline{\rho}\tilde{\dot{w}} = \frac{s_L^2}{4(\overline{D} + D_{t,t})}\rho_u \tilde{c}(1-\tilde{c}) + \rho_u U_{t,t}|\nabla c| \tag{4.36}$$

where $U_{t,t}$ is the transient turbulent velocity given by,

$$U_{t,t} = Au'Da^{1/4}\left\{1 + \frac{\tau'}{t_{fd}}\left[exp(-\frac{t_{fd}}{\tau'} - 1\right]\right\}^{1/2} \tag{4.37}$$

The above equation still does not account for ignition modelling, and is not reduced to laminar flame theory when $u' \to 0$, but the laminar source term is not zero. Also theoretically it gives asymptotically fully developed turbulent flames.

4.4 Thermal radiation modelling

The discrete ordinates (DO) radiation model solves for the radiation transfer equation. Two implementations of the DO model are available in FLUENT, uncoupled and energy coupled. The uncoupled DO model equation is used in this work. The uncoupled implementation is sequential in nature, i.e. the equations for the energy and radiation intensities are solved one by one, assuming prevailing values for other variables.

4.5 Physical properties

As the flame propagates in a closed vessel, the unburned gas ahead of the flame is compressed, thereby leading to an increase in pressure and temperature. The laminar burning

velocity is known to be dependent upon the pressure and temperature. Its general expression is defined by [8].

$$\frac{s_l}{s_{l0}} = (\frac{T_u}{T_{u0}})^m (\frac{p}{p_0})^n \tag{4.38}$$

According to the adiabatic compression laws:

$$\frac{\rho}{\rho_0} = (\frac{p}{p_0})^{-(1/\gamma)} \qquad \frac{\rho}{\rho_0} = (\frac{T}{T_0})^{-(1/\gamma - 1)} \tag{4.39}$$

i.e.,

$$(\frac{T}{T_0}) = (\frac{p}{p_0})^{(\gamma - 1/\gamma)} \tag{4.40}$$

As the pressure and the temperature do not react independently but change simultaneously, hence the laminar burning velocity can be rewritten as:

$$\frac{s_l}{s_{l0}} = (\frac{p}{p_0})^{n + m((\gamma-1)/\gamma)} = (\frac{p}{p_0})^{\epsilon} \tag{4.41}$$

where ϵ is the overall thermokinetic index, $\epsilon = n + m((\gamma - 1)/\gamma)$.
The unburned density, thermal diffusivity, and the molecular mass diffusivity are accounted for compressibility effects by [8]

$$\rho_u = \rho_{u,0} (\frac{p}{p_0})^{1/\gamma} \tag{4.42}$$

$$\alpha_u = \alpha_{u,0} (\frac{T}{T_0})^a (\frac{p}{p_0})^b \tag{4.43}$$

$$D = D_0 (\frac{T}{T_0})^c (\frac{p}{p_0})^d \tag{4.44}$$

Here, $\rho_{u,0}$ is the initial density, $\alpha_{u,0}$ and D_0 are the initial unburned thermal diffusivity and the molecular mass diffusivity at pressure p_0 and temperature T_0, respectively. a, b, c and d are the temperature and pressure coefficients for thermal diffusivity and molecular diffusivity.

4.6 Ignition modelling

Ignition is carried out by patching $\tilde{c} = 1$ (which signifies a burnt region) and a high temperature in a small circular region at the center (see Fig. 4.1). When a premixed mixture in a turbulent flow environment is ignited, a laminar flame propagates for a short time until the flame interacts with turbulence. Thus, the radius of this region represents the distance traveled by the flame before it interacts with turbulence and starts turbulent flame propagation.

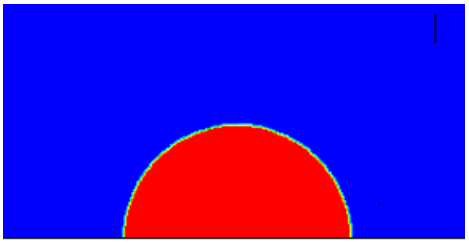

Figure 4.1: Graphical representation of the initial ignition patching of burned gas region at the start of the CFD simulation. BLUE represents the unburned gas region and RED represents the burned gas region.

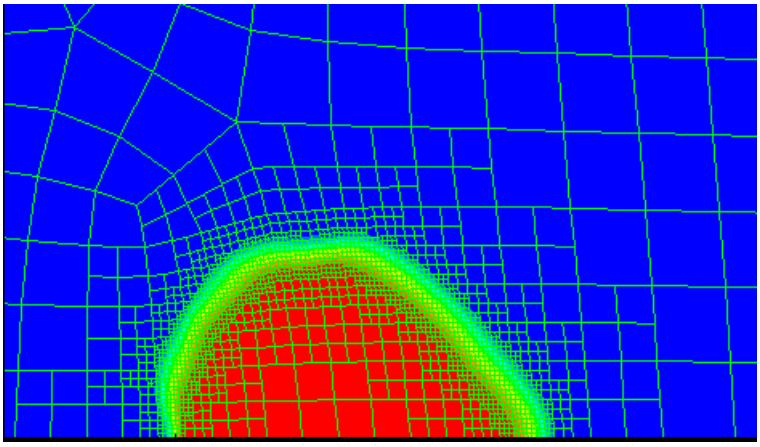

Figure 4.2: Graphical representation of the adaptive grid refinement. BLUE represents the unburned gas region and RED represents the burned gas region. The grid is more refined in the region of flame brush and coarser in the region of unburned and burned gas.

4.7 Adaptive grid refinement

Sathiah et al. [30] stress on the importance of grid refinement studies to capture the flame propagation properties accurately. They proposed to resolve the mean flame brush thickness with a dynamic adapting grid. Thus, the grid between $\tilde{c} = 0.1$ and $\tilde{c} = 0.9$ is dynamically resolved at every iteration. And thus, the mesh size is variable throughout the simulation process.

4.8 Applied Numerical Schemes

The commercial software ANSYS FLUENT (2008) is used for CFD simulations. Sathiah et al. [30] showed that density based solver give better results than pressure based solver. Thus, we use density based solver for our simulations. It solves Eq. 4.15 to 4.17 simultaneously as a set of equations. Equations for turbulent kinetic energy and dissipation rate i.e., Eq. 4.22 and 4.22 are solved sequentially. Within the density based solver, two algorithms are available for solving the coupled set of equations, namely, the coupled time-explicit formulation and the coupled time-implicit formulation. The coupled time-explicit

formulation is used as it was numerically more stable. The code employs a 4-stage Runge-Kutta scheme for time integration of the unsteady flows. The time step in this method is determined by the Courant-FriedrichsLewy (CFL) condition. The spatial discretization of the convective terms for flow, species and turbulence equations are performed using a second-order upwind numerical scheme.

4.9 CFD codes used in the past

CFD based simulations have been performed for a full scale containment of a Light Water Reactor (LWR) by Bielert et al. [19] and for a Boiling Water Reactor (BWR) by Manninen et al. [20]. Baraldi et al. [22] use the eddy-dissipation concept to model hydrogen combustion. This model does not account for initial laminar flame propagation and assumes that the burning rate is solely controlled by turbulence. The model is implemented in their in-house code REACFLOW [23]. The code is validated against hydrogenair flame propagation experiments, which were conducted in a tunnel [21] and in a closed cylinder [24].

Molkov et al. [25] proposed a model to simulate hydrogenair flame propagation based on the progress variable approach. This model accounts for initial laminar flame propagation and uses a gradient type source term to model the reaction or burning rate. The model takes into account the effects of turbulence on the flame propagation, the generation of turbulence in the flame front, and includes a fractal like flame wrinkling mechanism. It also takes preferential diffusion into account, which is important for hydrogenair combustion. In addition, the model also accounts for burning velocity dependence on pressure and temperature. This model is implemented in the commercial CFD code ANSYS FLUENT(2008) using UDFs. The model is validated against hydrogenair flame propagation experiments conducted in an open atmosphere [26], in a tunnel [27], in a vehicle refueling environment [28], in a closed cylinder [24], and in a vessel with pressure relief vents [29]. However, Molkov used LES for turbulence modelling with coarser grids. And they did not demonstrat that the grids used are adequate for LES type simulations.

The COM3D code is developed at Forschungszentrum Karlsruhe (FZK). The code solves the 3D unsteady, compressible NavierStokes equations using the standard $k\epsilon$ turbulence model. A modified eddy-break up combustion model, which is an extension of the standard eddy-break up model proposed by Spalding (1971), is implemented in COM3D. This model takes into account the distinction between movement of flamelets and turbulence itself. Kotchuorko (Makarov et al., 2010) extended the COM3D code and implemented the CRiteria and Experimentally Based COmbustion model (CREBCOM) proposed by Efimenko and Dorofeev (2001) for flame tracking. The burning rate constant is determined by the turbulent flame speed obtained from the Kawanabe correlation (Kawanabe et al., 2008). This model also accounts for dependence of the burning velocity on temperature and pressure. .

FLame ACceleration Simulator (FLACS) is a CFD code developed by GexCon since 1980. The code solves the unsteady compressible NavierStokes equation on a 3D Cartesian grid. Two different combustion models are implemented in FLACS: (a) flame model and (b) a simple interface model as described in Arntzen (1998). In the flame model, the flame brush thickness is artificially increased to capture the flame thickness in a coarse grid. In

the latter approach, the flame is treated as an interface between reactants and products. Both these combustion models use a submodel for the turbulent burning velocity (Arntzen, 1998) which consists of: (a) a laminar burning velocity expression that describes it as a function of gas mixture, fuel concentration, temperature, pressure, oxygen concentration in the air, and amount of inert diluents, (b) a submodel, which describes the first phase of flame propagation after ignition as quasi-laminar combustion, and (c) a submodel that the describes the turbulent burning velocity as a function of the turbulence intensity and length scale.

Chapter 5

Results

5.1 ENACCEF experiment 153 analysis

In this section the validation study analysis for the ENACCEF RUN-153 experiment is presented. The description of the experimental facility and initial conditions have already been described in Section 3.1. For the convenience of the reader, these are also given in Table 5.1.

Table 5.1: Initial Condition for ENACCEF RUN-153 experiment

Initial Temperature	296K
Initial Pressure	100kPa
Hydrogen concentration	13% by vol.

The commercial software GAMBIT has been used to create a two dimensional, axisymmetric geometry of the ENACCEF facility. The control volume is divided into 9600 hexahedral cells. The URANS approach is used to solve the compressible mass, momentum, energy, and progress variable equations using commercial software FLUENT. The two equation $k-\epsilon$ turbulence model is used to model turbulent Reynolds stresses. The combustion model is implemented through the in-house User Defined Functions (UDF) for FLUENT developed by NRG. The time step is determined using a CFL number of 0.8. In the subsequent subsections, the results of Zimont and Lipatnikov combustion model for the ENACCEF RUN-153 experiment are presented. Furthermore, the effect of heat loss due to radiation on flame propagation is examined. The validation criteria are based on the the flame position and pressure development as functions of time in the test facility. The flame position is determined corresponding to $\tilde{c} = 0.5$ as also used by Sathiah et al. [30] [8] and Gubba et al. [31]

5.1.1 Validation analysis using Zimont combustion model

Grid independence studies for this case have been performed by Sathiah et al. [8] and therefore have not been repeated. A base grid of 9600 hexahedral cells and two levels of adaptive grid refinement were found sufficient to capture the flame properties. The flame position is determined at the axis of the facility by progress variable $\tilde{c} = 0.5$.

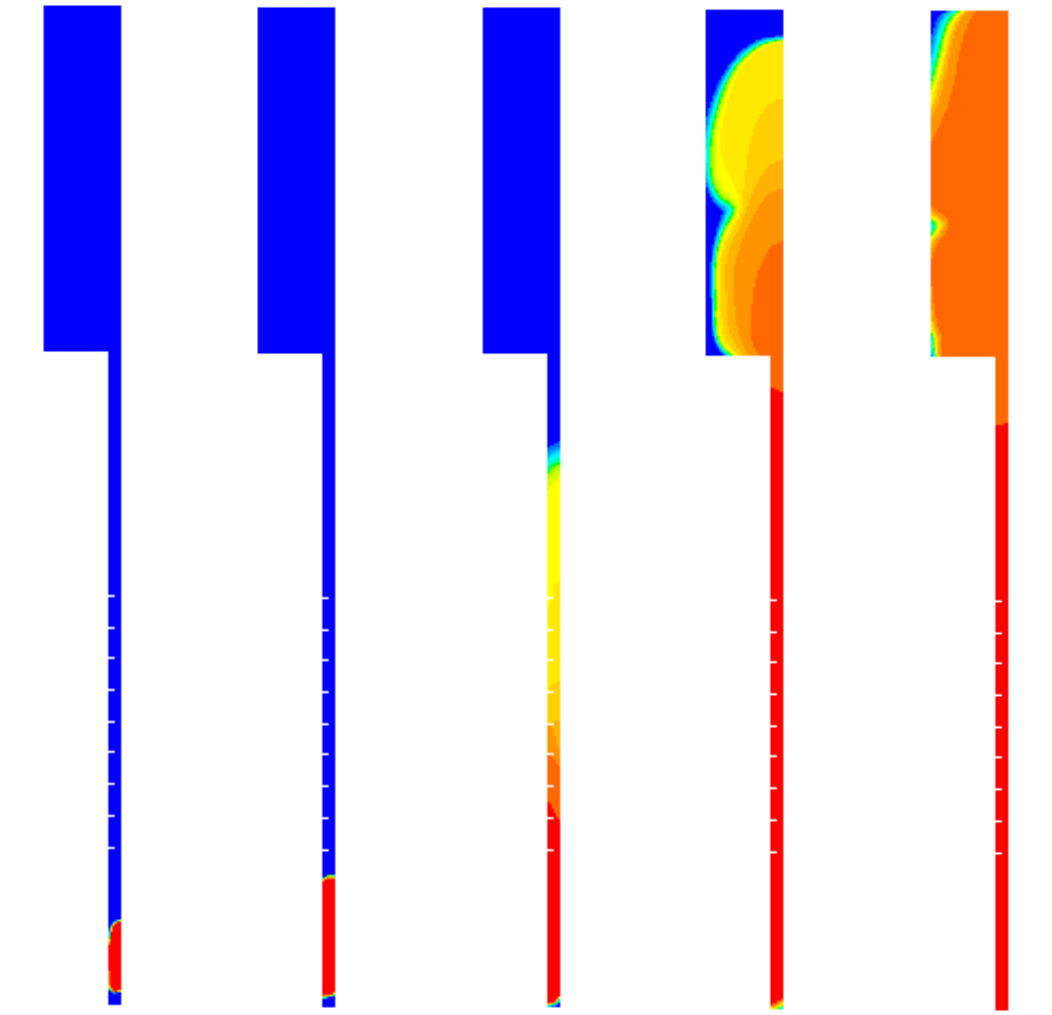

(a) $t = 0.014s$ **(b)** $t = 0.024s$ **(c)** $t = 0.036s$ **(d)** $t = 0.045s$ **(e)** $t = 0.054s$

Figure 5.1: Progress variable contours in ENACCEF RUN-153 using Zimont combustion model. BLUE reperesents the unburned gas region and RED denotes the burned gas region.

In Fig 5.1 we show the progress variable contours at different simulation times. These contours qualitatively indicate the extent of burned mixture. The flame propagation can be divided into 4 phases: 1) the quasi-laminar flame 2) the accelerating flame 3) the decelerating flame and 4) the jet flame. These phases can be seen in Fig. 5.2. In the first phase, the flame propagates in a quasi-laminar state from ignition at $t = 0$ till the time it reaches the first baffle at $t = 0.025s$. The flame brush thickness is very thin during this phase as can be seen in Fig. 5.1a & 5.1b. The flame velocities are over predicted

, as compared to the experiment, in this regime. The reason of over-precition could be 1) the presence of a lower level of intial turbulence than what we have assumed, 2) the over prediction of turbulence levels by the standard $k-\epsilon$ turbulence model, or 3) over prediction of the turbulent source term by the Zimont combustion model. The second phase of flame propagation starts when the flame reaches the first baffle. It encounters high turbulence generated by the baffles. The turbulence wrinkles the flame surface and increases the turbulent transport of heat and mass across the flame front. Therefore, the flame is accelerated and the flame brush thickness is increased. In Fig. 5.2a, we see that for this phase, the second phase, the axial flame position and the slope of the axial flame position are well predicted by the CFD simulations as compared to the experimental results. In the CFD simulation the flame reaches the last baffle at $t = 0.033s$. After this the flame stops accelerating, and the deceleration of the flame starts. This can be recognized as phase three. This deceleration phase lasts till the flame reaches the end of the acceleration tube, i.e. at $t = 0.042s$. In this phase, the flame velocity is decreased due to lower turbulence levels. Finally, in the fourth phase, the flame enters the dome where it slowly consumes the remaining unburnt gasses.
The development of pressure in the EN-153 is shown in Fig. 5.2b. During the quasi-laminar and acceleration phase we have negligible pressure rise. While the flame is accelerating, compression waves are generated from the flame front which travel towards the dome entrance. At the entrance of the dome, these waves are reflected back as expansion waves. These expansion waves create a sudden decrease pressure which results in the intermediate pressure peak. After this intermediate peak, the flame is already inside the dome, and the pressure rises rapidly as the unburnt gasses in the dome are burnt. The end pressure is at Adiabatic Isochoric Complete Combustion (AICC) value since, we have not considered the heat loss from experimental facility. In Fig. 5.2d we see that both the velocity peaks are captured. The magnitude of the first pressure peak is over predicted and the second pressure peak is under predicted. A quantative difference of pressure values between the experiment and the CFD simulation is given in Table 5.2. The first peak pressure is slightly over predicted by 5.13%. The maximum peak pressure is over predicted by 6.24%. The pressure rise dp/dt until the intermediate peak is under predicted by 16%. The pressure rise dp/dt until the second peak is significantly under predicted by 67.5%.

Table 5.2: Quantative error in Zimont combustion model

	Experiment	Zimont model	Error %
First Peak Pressure	2.493e+05	2.621e+05	5.13%
Maximum peak pressure	4.5643e+05	5.296e+05	6.24%
First rate of pressure rise dp/dt	3.5929e+09	3.017e+09	-16%
Second rate of pressure rise dp/dt	2.2811e+09	7.412e+08	-67.5%
First eigen frequency	226.3	231.6	2.34%
Amplitude first eigen frequency	5455	5221	-6.11%

The structure of the experimental facility has an eigen frequency. If the pressure oscillations coincide with this frequency they can cause resonance of the experimental facility which can affect the structural integrity of the facility. Hence, it is important to predict the frequency of oscillations in the combustion process. Fast Fourier Transform was per-

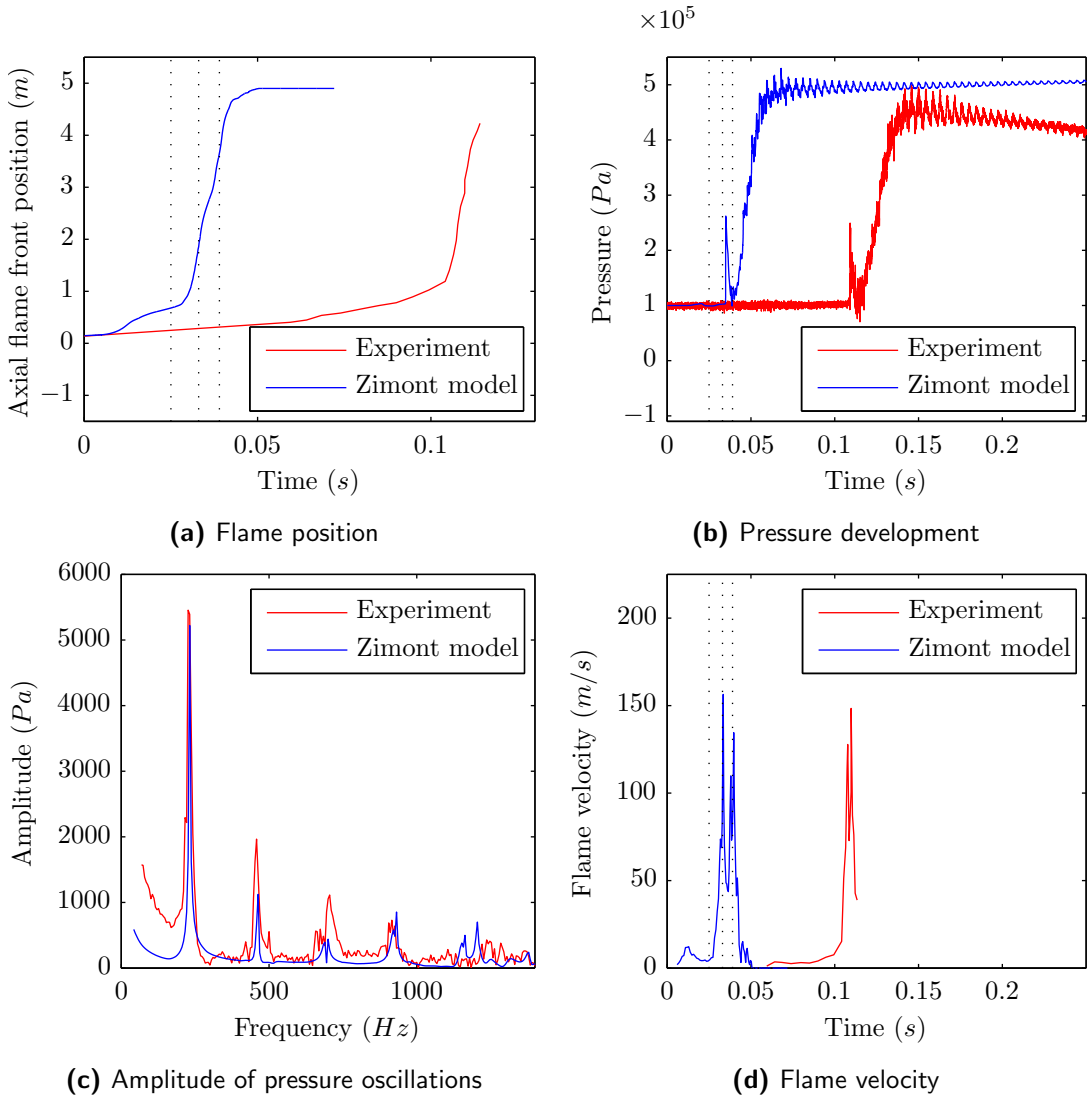

(a) Flame position

(b) Pressure development

(c) Amplitude of pressure oscillations

(d) Flame velocity

Figure 5.2: Validation analysis for ENACCEF RUN-153 experiment using Zimont combustion model

formed to analyze the frequency of the pressure oscillations in the EN-153 experiment. We can see in Fig. 5.2c that the first eigen frequency is captured at $231.6Hz$, with an error of 2.34% with an under prediction of 6.11% in amplitude of pressure oscillation.

5.1.2 Validation analysis using Lipatnikov combustion model

In this section we present the validation results using the Lipatnikov combustion model. In Fig 5.3 we present the progress variable contours, using the Lipatnikov combustion model, at different simulation times. A base grid of 9600 hexahedral cells, same as that of previous section, was used. The validation results are shown in Fig. 5.4. Two levels of adaptive grid refinement were found sufficient to capture the flame propagation properties. The flame position is determined at the axis of the geometry corresponding to the progress variable value $\tilde{c} = 0.5$.

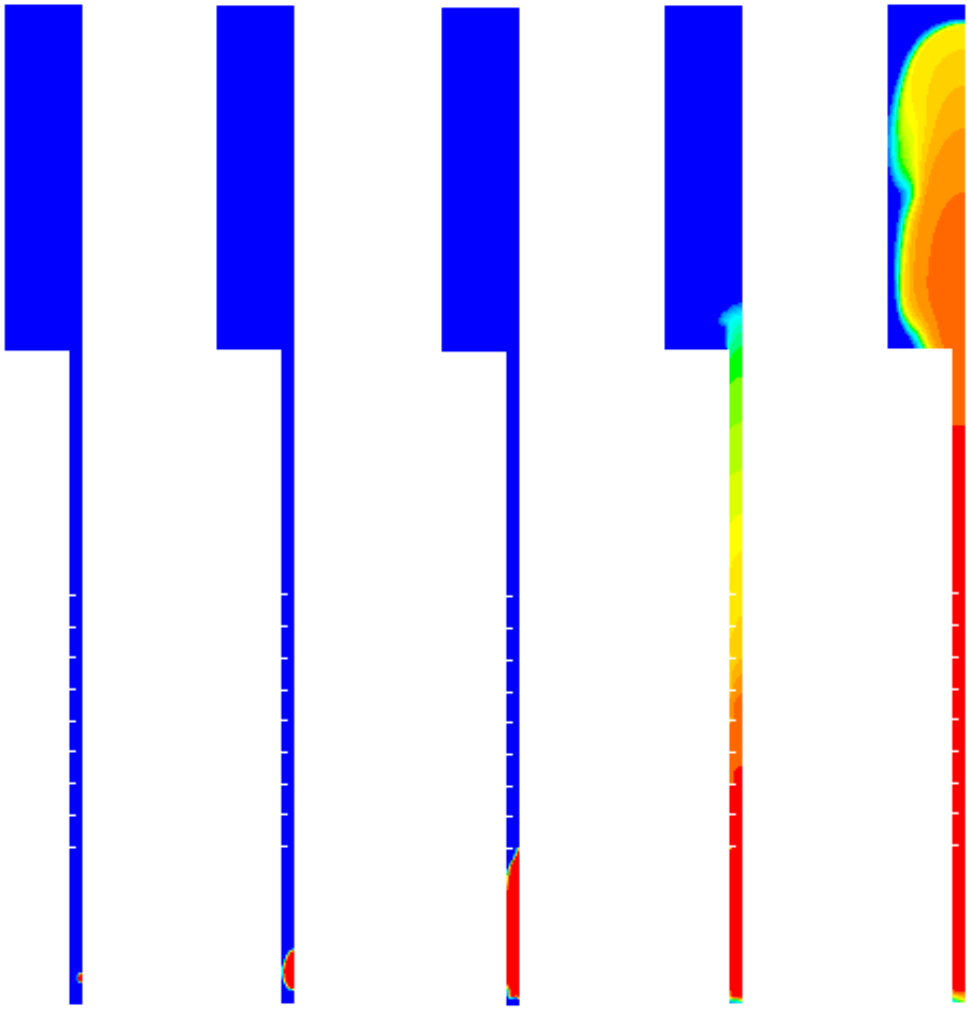

(a) $t = 0.015s$ **(b)** $t = 0.035s$ **(c)** $t = 0.055s$ **(d)** $t = 0.065s$ **(e)** $t = 0.075s$

Figure 5.3: Progress variable contours in ENACCEF RUN-153 using Lipatnikov combustion model. BLUE reperesents the unburned gas region and RED denotes the burned gas region.

The flame propagation in the four phases has already been discussed in the previous section. We will analyze the results on the same line. In this case, the Lipatnikov combustion model, we can see in Fig. 5.3 that the flame reaches the first baffle at $t = 0.055s$ in the CFD simulations. That is, the flame propagation in the first phase, i.e. the quasi-laminar stage, is much slower. The relatively low flame velocity is due to the consideration of the

transient quasi-laminar flame propagation in the low turbulence regime. However, the flame velocity is still over predicted as compared to the experiment (see Fig. 5.4a). The possible reasons for over prediction of flame velocity, already discussed in previous section, are 1)higher assumed initial turbulence levels 2)over prediction of turbulence by the standard $k-\epsilon$ turbulence model, or 3) still the over predicted source term in the progress variable equation. During the second phase, the acceleration phase, the flame position and slope of the flame position are well predicted by the CFD simulations, as compared with experimental results (see Fig. 5.4a). The flame reaches the last baffle at $t = 0.061s$ when the decelaeration phase starts. The fourth phase starts at $t = 0.065$ when the flame reaches the dome and slowly burns the unburnt gasses present in the dome.

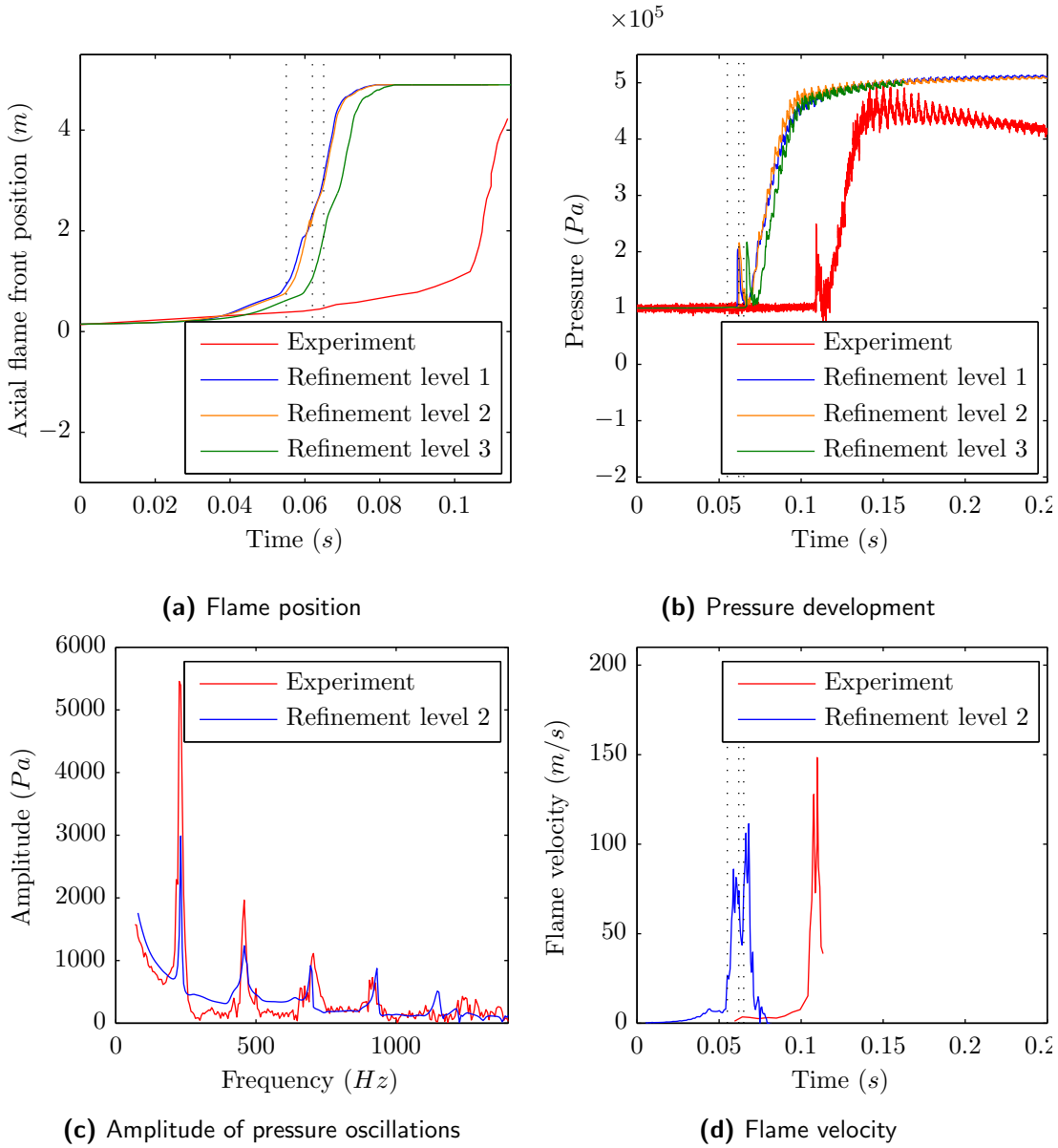

(a) Flame position

(b) Pressure development

(c) Amplitude of pressure oscillations

(d) Flame velocity

Figure 5.4: ENACCEF Run-153 validation results from the Lipatnikov combustion model

The pressure development for Lipatnikov combustion model is shown in Fig. 5.4b. There is no significant pressure rise during the quasi-laminar and acceleration phase. The intermediate peak due to the reflected expansion wave is well captured in the CFD simulation, however the value of this pressure peak is under predicted in comparison with experiments. After this the flame is already in the dome and the pressure rises rapidly due to burning of the remaining unburnt gasses. The peak pressure is at AICC values because no heat loss from the walls of experimental facility is assumed. The amplitude of pressure oscillation near the point of complete combustion is less well predicted. The quantitative differences in the pressure values of the experiment and CFD simulations are presented in Table 5.3. The first pressure peak is under predicted with an error of 13.4%. The maximum peak pressure is over predicted by 12.28%. The pressure rise dp/dt until the first pressure peak is under predicted by 54.77%. The pressure rise dp/dt until the second pressure peak is over predicted by 91.04%.

Table 5.3: Quantative error in Lipatnikov combustion model

	Experiment	Lipatnikov model	Error %
First Peak Pressure	2.493e+05	2.159e+05	-13.4
Maximum peak pressure	4.5643e+05	5.1247e+05	12.28
First pressure gradient dp/dt	3.5929e+09	1.625e+09	-54.77
Second Pressure Gradient dp/dt	2.2811e+09	2.043+08	-91.04
First eigen frequency	226.3	231.6	2.34
Amplitude first eigen frequency	5455	2987	-45.24

The frequency of pressure oscillations is again determined using Fast Fourier Transform (see Fig. 5.4c). The first eigen frequency is predicted at $231.6Hz$ with an error of 2.34%. The amplitude of pressure oscillation at this frequency is under predicted by 45.24%.
In Fig. 5.4d we the velocity profile for axial flame position. Both velocity peaks are captured, and in the author's opinion the velocity profile is qualitatively well predicted. However, quantitatively, the magnitud of both the velocity peaks is under predicted.

Comparison between Zimont and Lipatnikov model

In this section we compare the performance of the Zimont and the Lipatnikov combustion model in the ENACCEF RUN 153 experiment.

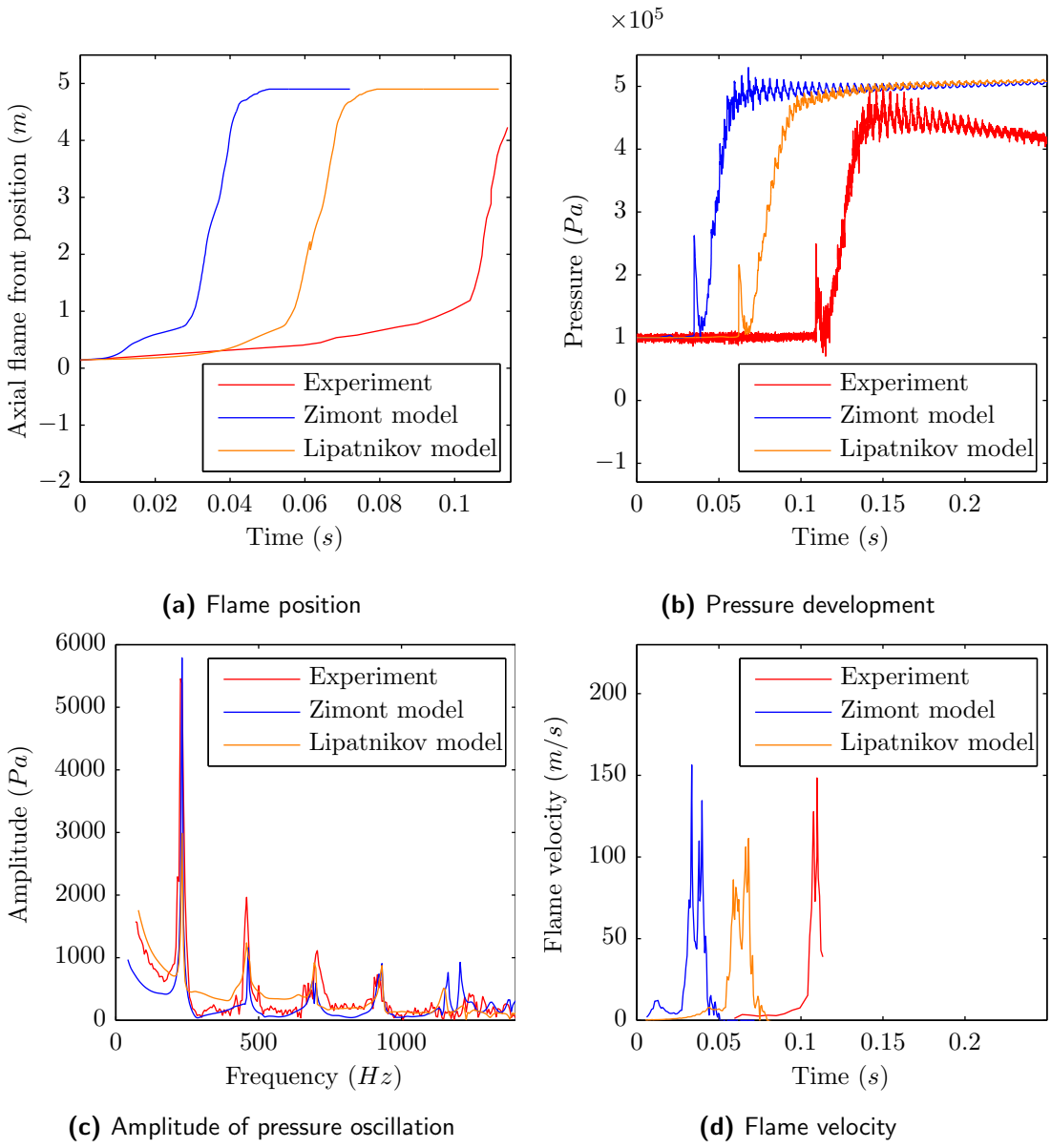

(a) Flame position

(b) Pressure development

(c) Amplitude of pressure oscillation

(d) Flame velocity

Figure 5.5: Comparison in ENACCEF RUN-153 experiment between Zimont and Lipatnikov combustion model

A comparison of the flame position obtained using the Lipatnikov and Zimont combustion model is shown in Fig. 5.5a. In the quasi-laminar phase the flame velocity predicted by the Lipatnikov combustion model is lower than the flame velocity for the Zimont combustion model. Thus, we see slow flame propagation in case of the Lipatnikov combustion model. This reduces the time shift between the CFD simulation and experiment. In the flame acceleration phase, i.e. in high turbulence regime, both the models are in good agreement

in terms of flame position and slope of the flame position. Finally, in the deceleration phase both models predict low burning velocities.

The comparison in pressure development using the Zimont and the Lipatnikov combustion model is shown in Fig. 5.5b. We see that, the intermediate peak pressure is slightly over-predicted by the Zimont combustion model, and slightly under predicted by the Lipatnikov combustion model. Furthermore, we see that the amplitude of the pressure oscillations just after complete combustion (near peak pressure) is under predicted by the Lipatnikov combustion model as compared to both the experiment and the Zimont combustion model. This under prediction of amplitude can be attributed to low burning velocities predicted by the Lipatnikov combustion model as compared to the experiment and the Zimont combustion model (see Fig. 5.5d). Also, in the velocity profiles of Fig. 5.5d, we see that for the Zimont combustion model the development of velocity peaks is sooner than in case of the Lipatnikov combustion model. This is due to the over predicted flame velocity in the quasi-laminar phase for the Zimont combustion model. Furthermore, we see that in experiments the magnitude of first velocity peak is less than the magnitude of second velocity peak. This trend has been observed in the Lipatnikov combustion model, but not in the Zimont combustion model.

Thus, we see that for the ENACCEF RUN-153 experiment, in the quasi-laminar phase, the Lipatnikov combustion model is predicting low flame velocity, less than the Zimont combustion combustion model, which is more in agreement with the experiment results. It is able to capture all the physical phenomena qualitatively. Though, in the acceleration and the deceleration phase it is predicting lower burning velocities than the experiment. This results in under prediction of the value of intermediate pressure peak and under prediction of the pressure oscillations (near peak pressure) just after complete combustion.

5.1.3 Validation analysis using Zimont model with radiation heat loss

Heat losses due to radiation effects could be important for combustion processes. Radiation heat losses could affect the pressure development in the facility, which in turn could affect the flame propagation. Low pressure means low laminar flame speed, see Eq. 4.38, and thus slow flame propagation. Therefore, DO radiation model is used to see the effect of thermal radiation heat losses from the experimental facility. The absorption coefficient of this model is determined by the in-house code of NRG. The Zimont model is used to model flame propagation because it is able to capture the high amplitude of oscillations just after complete combustion.

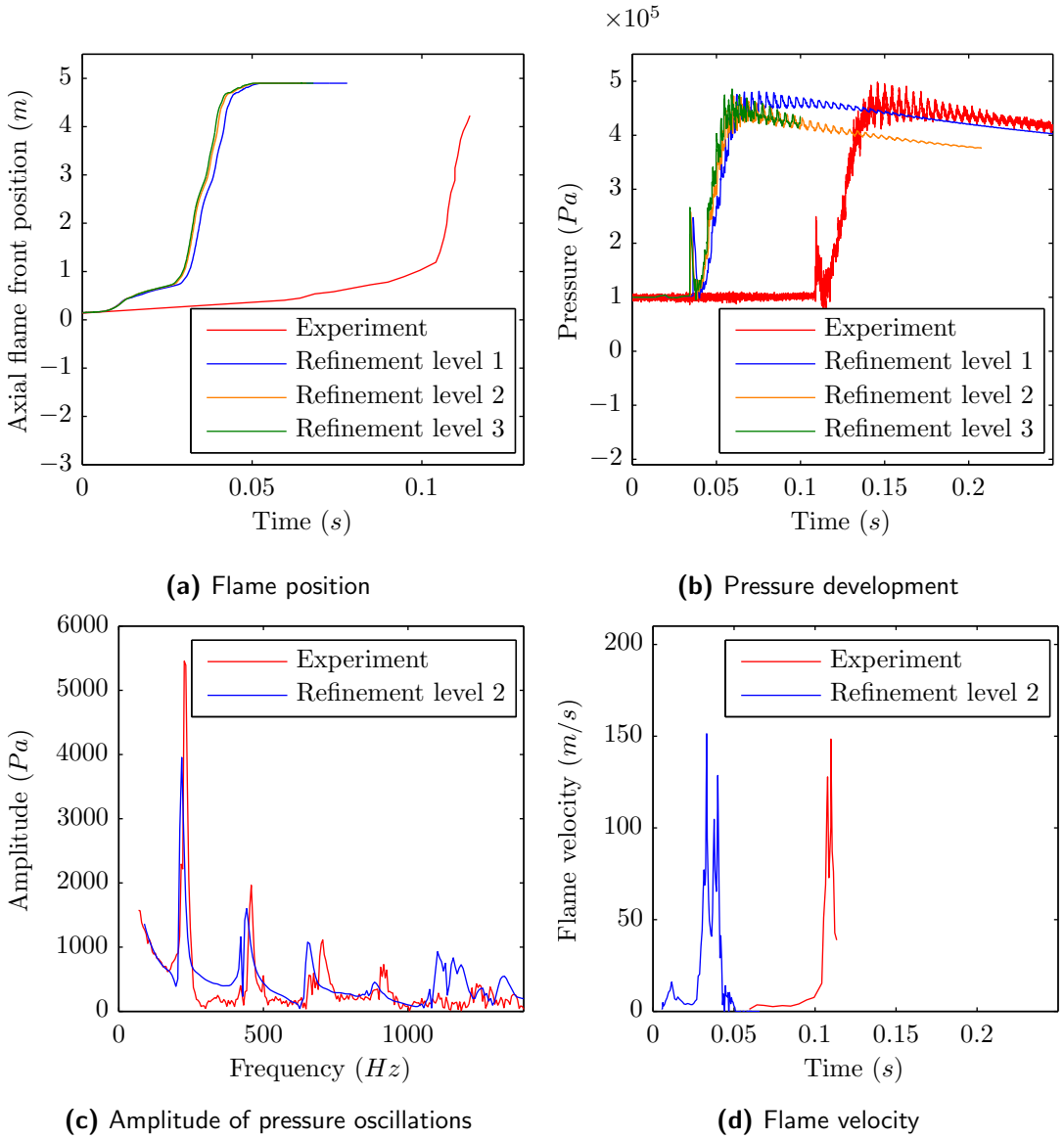

(a) Flame position

(b) Pressure development

(c) Amplitude of pressure oscillations

(d) Flame velocity

Figure 5.6: ENACCEF Run-153 validation analysis for Zimont combustion model with DO radiation heat loss

A base grid of 9600 cells is used. Grid independence tests with 1, 2 & 3 adaptive grid

refinement levels are shown in Fig. 5.6a & 5.6b. Two levels of refinement were found sufficient to capture the properties of flame propagation. In Fig. 5.6b, we observe that the first pressure peak is quite accurately captured. The peak pressure however is slightly under predicted. This could be due to the fact that exact thermal radial properties were not known, and reasonable values were assumed to see the effect of radiation heat loss on flame propagation. The decay in the pressure profile after complete combustion is also successfully captured due to thermal radiation effects. The slope of pressure decay in the CFD simulation is in reasonable agreement with that observed in the experiment. In Fig. 5.6c we can observe that the amplitude of the pressure oscillations is under predicted. This is due to lower values of the pressure amplitude predicted due to consideration of heat losses. In Fig. 5.6d we see the comparison of velocity profiles from the CDF simulation and the experiemnt. Both the velocity peaks are captured. However, the first velocity peak is over predicted in magnitude, and the second velocity peak is under predicted in magnitude.

Comparison between with and without radiation heat losses

In this section, we compare the flame propagation in the ENACCEF RUN 153 using the Zimont combustion model with and without thermal radiation heat losses.

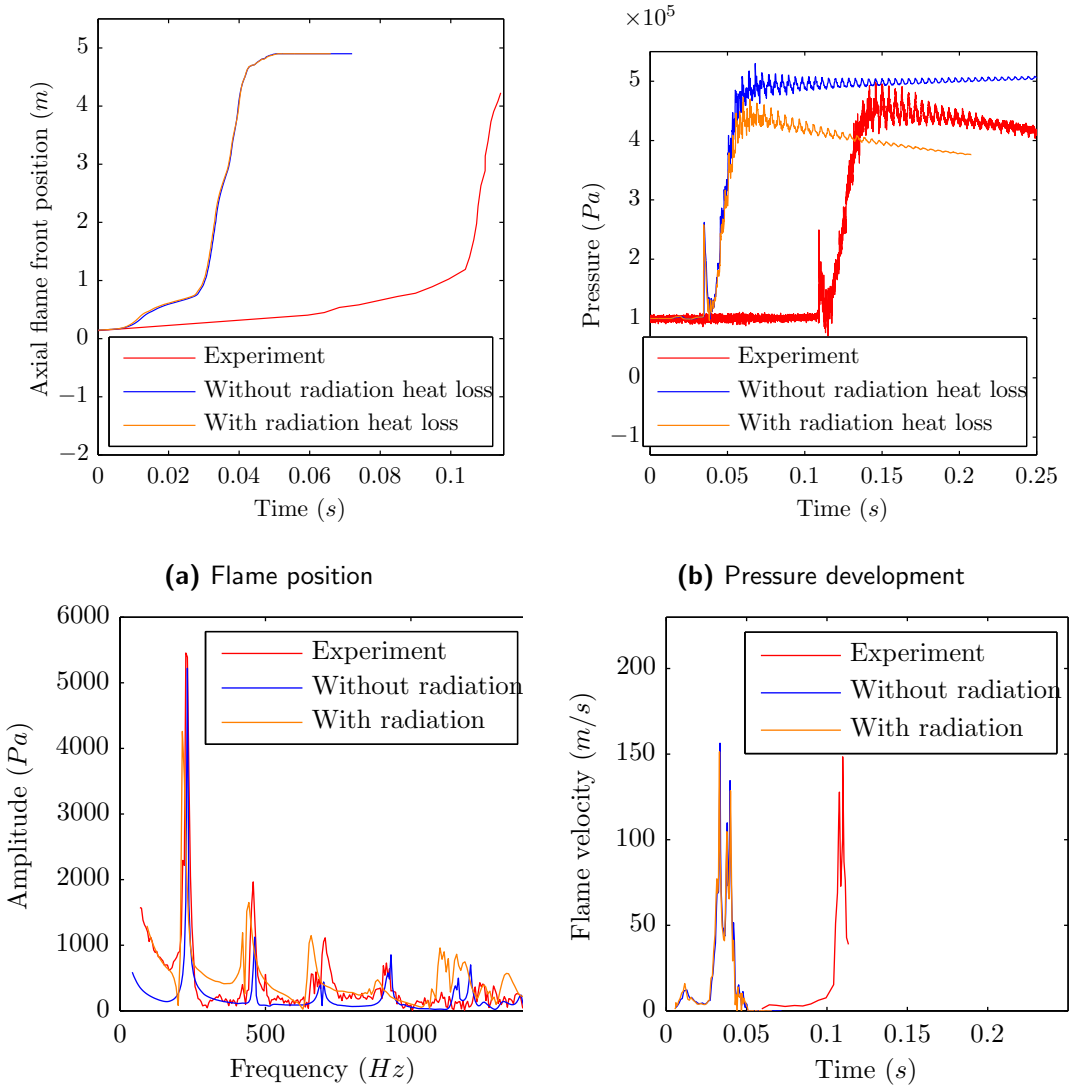

(a) Flame position

(b) Pressure development

(c) Amplitude of pressure oscillations

(d) Flame velocity

Figure 5.7: Comparison in ENACCEF RUN-153 experiment between Zimont combustion model with and without radiation heat loss

In Fig. 5.7a we see that heat loss due to radiation has negligible effect on the flame position or the slope of flame position. Therefore, also the flame velocity profile in Fig. 5.7d is similar for both the cases of, with and without, thermal radiation heat loss. In Fig. 5.7b we see that considering radiation heat loss is necessary to predcit the decay in pressure following complete combustion.

5.2 THAI experiment HD-12 analysis

In this section we present the validation results for the THAI HD-12 experiment. The description of the test facility and the experimental set-up has already been described in Section 3.2. For the convenience of the reader the initial conditions are once again specified in Table 5.4

Table 5.4: Initial Condition for THAI HD-12 experiment

Initial temperature	291K
Initial pressure	150kPa
Hydrogen concentration	8% by vol.

The commercial software GAMBIT is used to create a 2-D axisymmetric geometry of the THAI facility. The control volume is divided into 2000 hexahedral cells. A coarse mesh is used for preliminary analysis of the combustion models. A 2×2 refined mesh of the base grid, i.e. with 8000 cells is then used to ensure a robust grid independency analysis. These results have been shown in Appendix B.3. The URANS approach is used to solve compressible mass, momentum, energy and progress variable equations in the commercial software FLUENT. The $k - \epsilon$ turbulence model is used to model turbulent Reynolds stresses. Flame propagation is modelled using two different combustion models: 1) the Zimont combustion model [4] and, 2) the Lipatnikov combustion model. These models are implemented using the in-house UDF code developed by NRG. Additionally the effect of radiation heat loss on the flame propagation is shown. This has been implemented using the DO radiation model. The time step is determined using the CFL number of 0.8. The axial flame position and the pressure development in THAI facility are used to perform validation with experiments. The flame position is determined as in the case of experiments, that is, from the flame arrival at the 13 temperature sensors located along the axial direction.

5.2.1 Validation analysis using Zimont combustion model

In this section, we present the flame propagation results using the Zimont combustion model for the THAI HD-12 experiment. In Fig 5.8, we show the progress variable contours of the Zimont combustion model in the THAI DH-12 experiment. THAI is a vessel type test facility without any obstacles. The flame brush thickness is very thin at all simulation times. This indicates that the turbulent velocity fluctuations are weak and that they cannot penetrate the flame brush. Therefore, the turbulence levels are low and the velocity fluctuations are small. Thus, the flame is traveling in weakly turbulent region. Also we can see that the flame is propagating fast in axial direction than other regions. This trend that has also been observed in the experiments (see Fig. B.2).

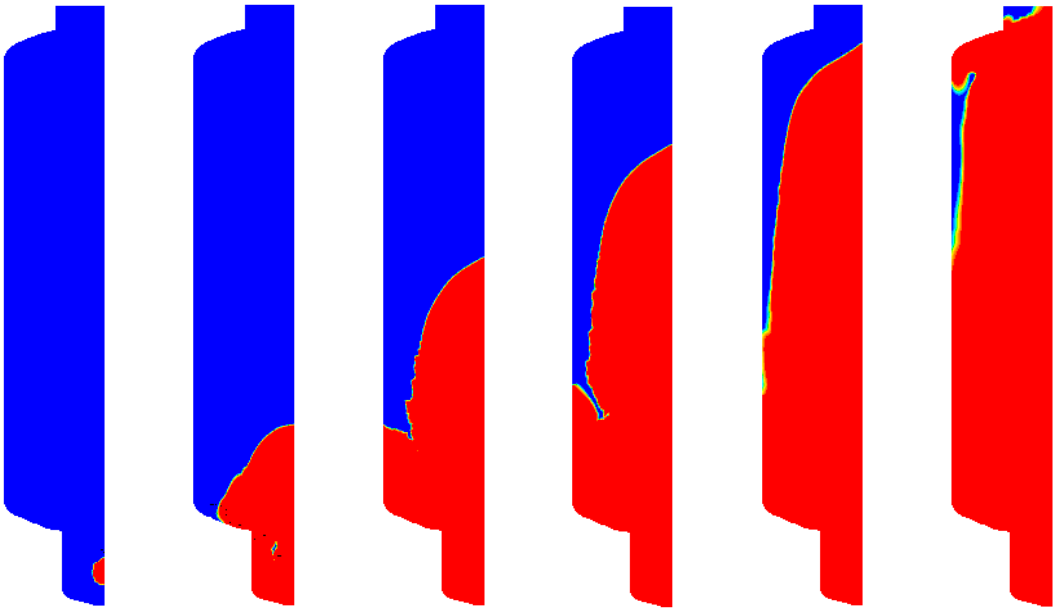

(a) $t = 0.12s$ **(b)** $t = 0.48s$ **(c)** $t = 1.02s$ **(d)** $t = 1.47s$ **(e)** $t = 1.96s$ **(f)** $t = 2.49s$

Figure 5.8: Progress variable contours in THAI HD-12 experiment using Zimont combustion model. BLUE reperesents the unburned gas region and RED denotes the burned gas region.

In Fig. 5.9 we present the validation analysis results using the Zimont combustion model for the THAI HD-12 experiment. Grid independence tests were performed and four levels of adaptive mesh refinement were found to be sufficient to capture the flame propagation properties. In Fig. 5.9a, we present the axial flame position as a function of time. We see that the flame position from the experiments is available from $t = 1.7s$ and not $t = 0s$. In the author's opinion a possible reason for this could be the time delay during the ignition process of the unburned mixture. In the CFD simulations, we observe that the flame is propagating very fast. This is further corroborated in Fig. 5.9c with flame velocity profiles of the experiment and the CFD simulation. In case of the experiment, the maximum velocity is $1.08m/s$, whereas the maximum predicted values in CFD simulation is as high as $3.07m/s$. Clearly the flame velocity is highly over predicted in the CFD simulation. The reason for this over-prediction of the flame velocities could be 1) presence of a lower initial level of turbulence than what we have assumed, 2) over prediction of the turbulence levels by the standard $k-\epsilon$ turbulence model, or 3) over prediction of the turbulent source

term by the Zimont combustion model in the progress variable equation.

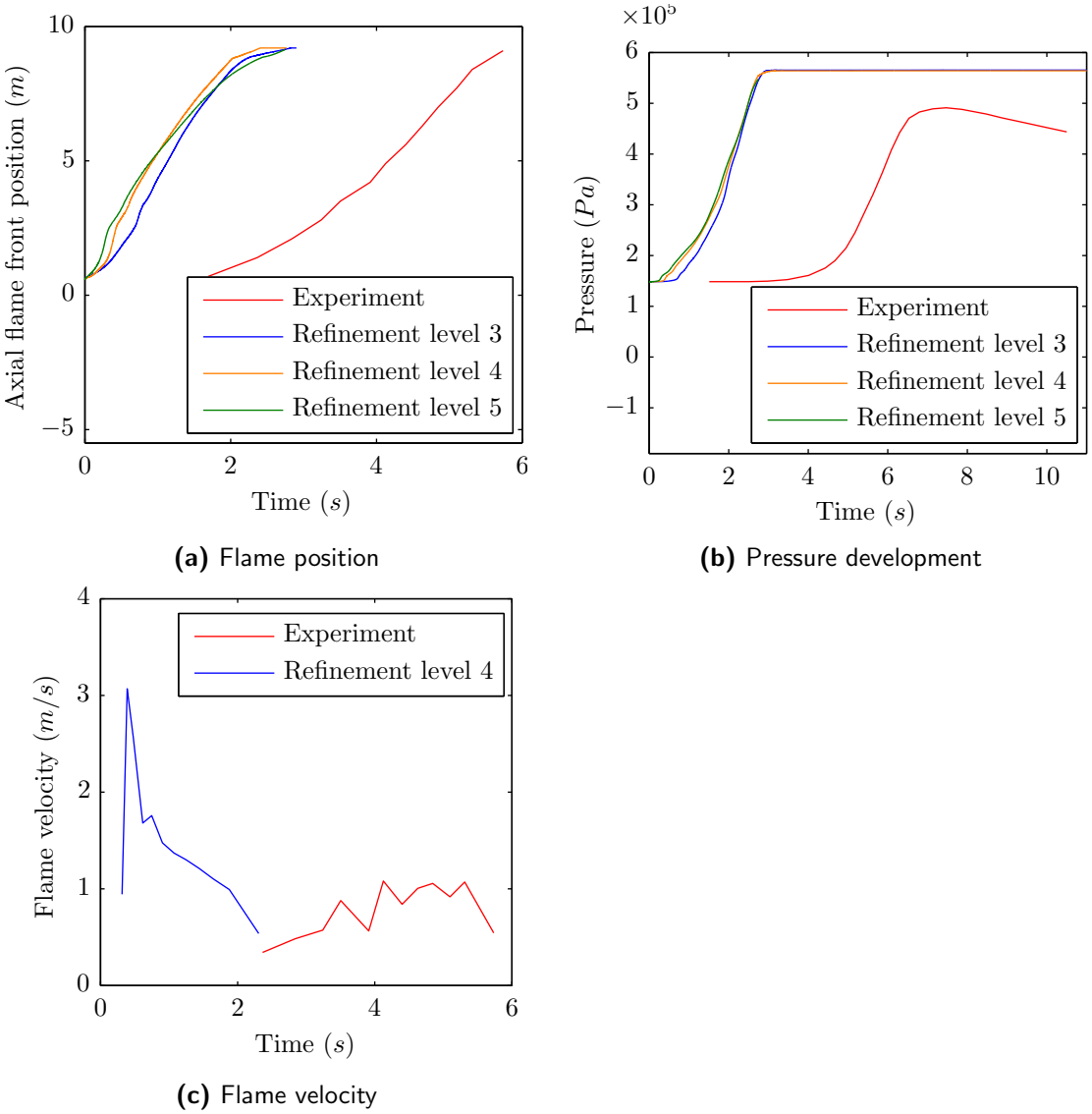

(a) Flame position

(b) Pressure development

(c) Flame velocity

Figure 5.9: Validation results in THAI HD-12 experiment from Zimont combustion model

In Fig. 5.9b we can see the pressure development in the THAI HD-12 experiment using the Zimont combustion model. The almost linear pressure rise indicates that the burning rate is overestimated and that the burning rate does not change significantly during the combustion process. The peak pressure is at the AICC value since no heat loss is assumed from the walls of the test facility.

5.2.2 Validation using Zimont model without taking account of PDT instability effects

Some research groups, for eg. Hoyes et al. [32], perform the validation study for the THAI hD-12 experiment without considering the PDT instability effects. In Section 2.4, we extensively discussed the effect of PDT instabilities on the flame propagation. Furthermore, we have emphasized the importance of PDT instability for flame propagation in hydrogen-air mixtures. Therefore, taking the PDT instability factor into account in the CFD modelling of hydrogen-air flames is certainly very important. However, to see the effect of PDT instability on the flame propagation, CFD simulations without PDT instability effects were performed. The results for this computation are presented in this section.

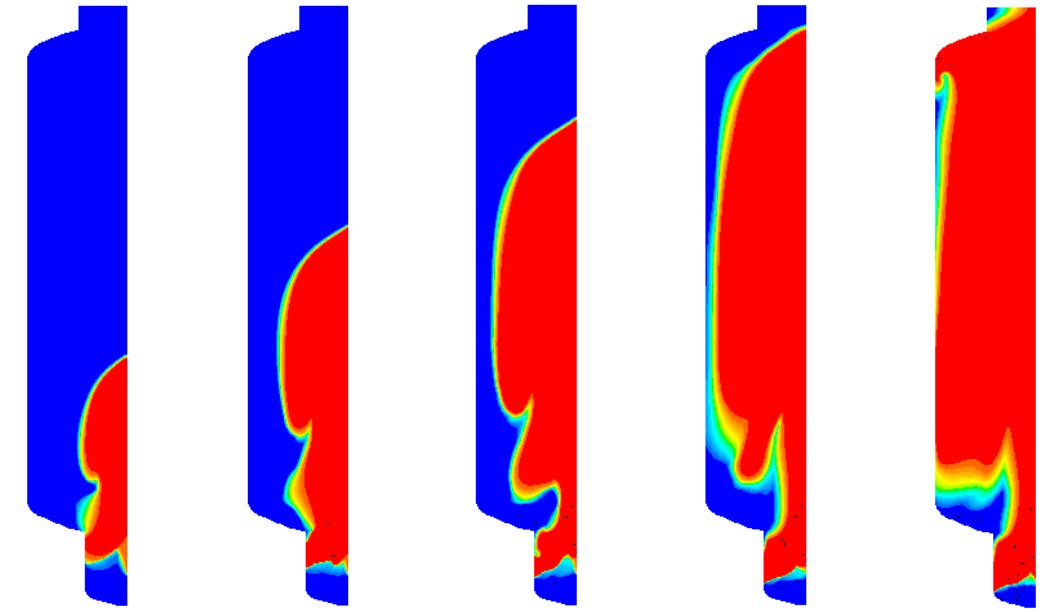

(a) $t = 1.50s$ **(b)** $t = 2.03s$ **(c)** $t = 2.51s$ **(d)** $t = 3.01s$ **(e)** $t = 3.51s$

Figure 5.10: Progress variable contours in THAI HD-12 experiment using Zimont combustion model without taking account of PDT instability effects

In Fig. 5.10 we show the progress variable contours of the Zimont combustion model without taking account of PDT instability effects. We observe that the flame brush is slightly thicker in this case, as compared to the case of Zimont combustion model with PDT instability effects (see Fig. 5.8). The flame propagation is fast along the axial direction, a trend also observed in experiments. The flame propagation in the downward direction i.e. below the ignition region is almost negligible, and the gasses in this region are burned only when the process is nearing complete combustion.

The validation analysis for the THAI HD-12 experiment using the Zimont combustion model without PDT instability effects is presented in Fig. 5.11. Three levels of adaptive grid refinement were found to be sufficient in order to capture the flame propagation dynamics.

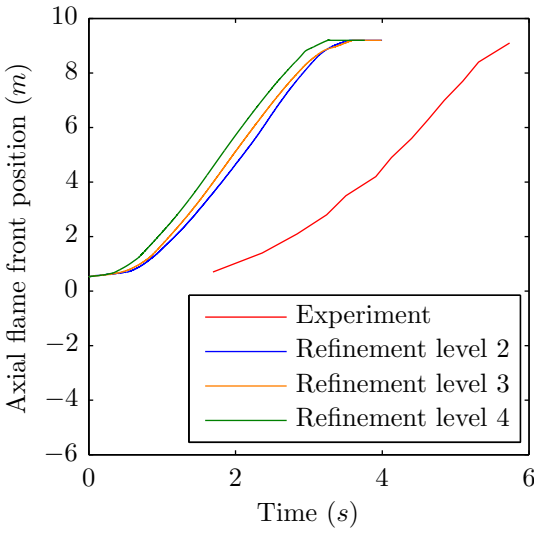

(a) Flame position

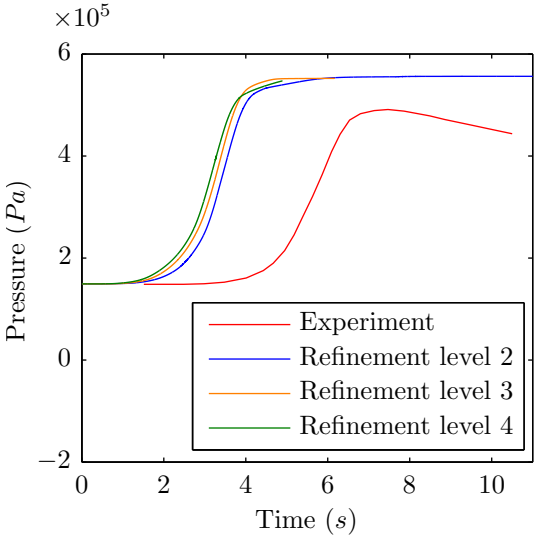

(b) Pressure development

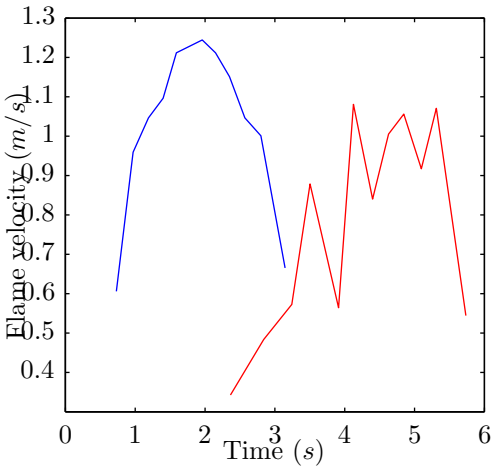

(c) Flame velocity

Figure 5.11: Validation results in THAI HD-12 experiment using Zimont combustion model without taking account of PDT instability effects

The flame position as a function of time is shown in Fig. 5.11a. The possible reason for abnormalities in the experimental data of the flame position, i.e. ignition delay, has already been discussed in the previous section. In the CFD simulations, we see that flame profile is reasonably well captured. The slope of the flame position in the CFD simulation is steeper than that observed in the experiment. This indicates higher flame velocities predicted by the CFD simulation.

In Fig 5.11c we see a comparison of flame velocities for the Zimont combustion model without PDT instability effects and the experiments. The CFD simulations have not been able to capture the flame velocity profile of experiments. However, the magnitude of the flame velocities in both the cases is quite close. The maximum velocity obtained in CFD simulations is $1.24 m/s$, and the corresponding value in experiments is $1.08 m/s$. The

possible reasons for higher predicted flame velocities has already been discussed namely 1) presence of lower turbulence levels than what we have assumed, 2) over prediction of turbulence levels by $k - \epsilon$ turbulence model, or 3) over prediction of source term in progress variable equation by the Zimont combustion model.
In Fig 5.11b we show the pressure development in THAI HD-12 experiment. Due to exclusion of PDT instability effects, the turbulent flame speed assumes lower values. Thus, the unburnt gasses are burnt slowly and the rise in pressure is very slow and gradual. The slope of pressure profile from CFD simulations is much more in agreement with experiments. Since no heat loss from experimental facility is assumed the end pressure is obtained at AICC values.

Comparison of Zimont model with and without PDT

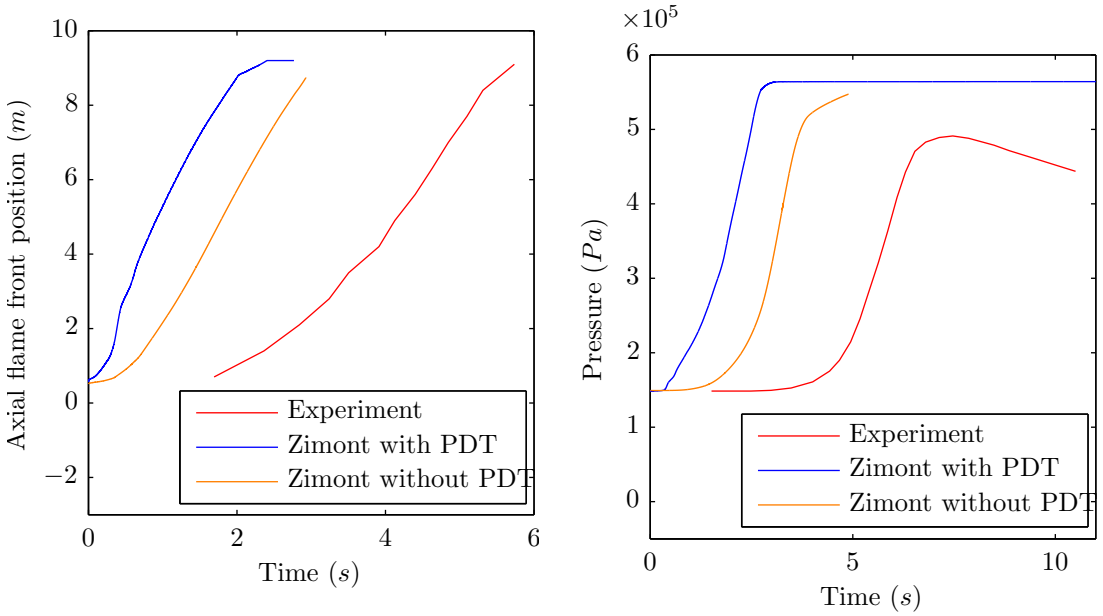

(a) Flame position **(b)** Pressure development

Figure 5.12: Comparison of flame properties in THAI HD-12 experiment for Zimont combustion model with and without PDT effects

In Fig 5.12 we compare the flame properties from the Zimont combustion model with PDT effects, and the Zimont combustion model without PDT effects. We see that for both the flame position and pressure profile, the Zimont model without PDT effects is much more in agreement with experiments. However, there are two errors that should be emphasized: 1) The Zimont mcombustion model is used outside it's regime of validity, and 2) PDT instability effects are excluded whereas in reality they are very important especially for low concentration hydrogen-air mixtures. These two errors are opposite in nature, i.e. the Zimont model over predicts the turbulent flame speed and excluding PDT under predicts the turbulent flame speed. Thus, they offset each others effect and we obtain good results. However, strictly speaking this method is wrong, and thus, should NOT be used.

5.2.3 Validation analysis using Lipatnikov combustion model

We know that the Zimont model is a purely turbulent combustion model and is valid for flame propagation of a completely developed turbulent flame. We know that the flame velocity in THAI HD-12 experiment is very low (see Fig. 5.11c) , and thus, the flame is travelling in a quasi-laminar regime. Therefore, CFD simulations using the Lipatnikov combustion model are performed in the THAI HD-12 experiment. The results for this simulation are presented in this section.

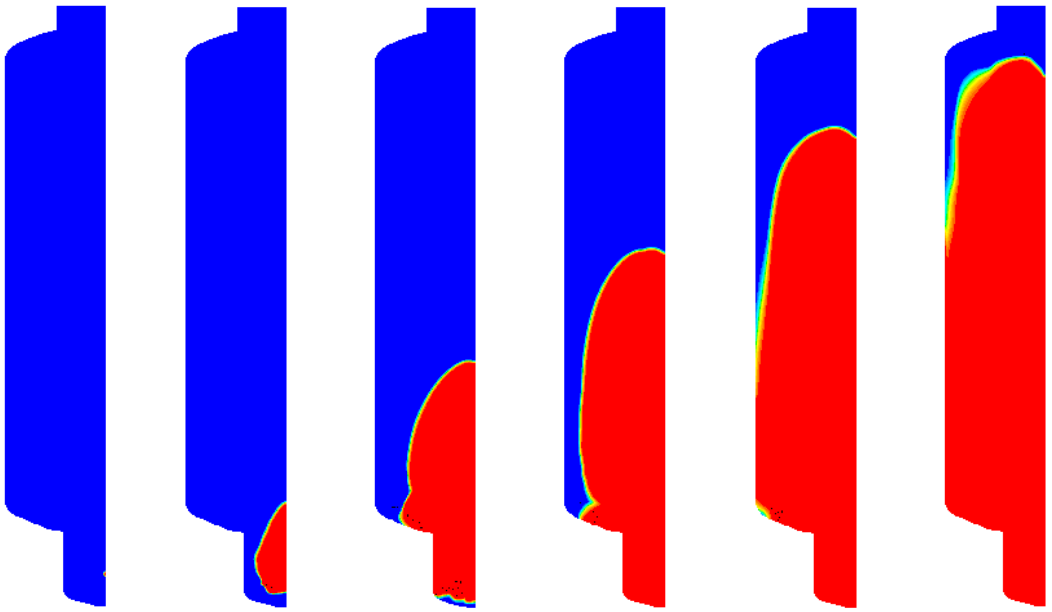

(a) $t = 0.11s$ **(b)** $t = 0.51s$ **(c)** $t = 1.04s$ **(d)** $t = 1.50s$ **(e)** $t = 2.03s$ **(f)** $t = 2.54s$

Figure 5.13: Progress variable contours for THAI HD-12 experiment using Lipatnikov combustion model. BLUE reperesents the unburned gas region and RED denotes the burned gas region.

In Fig 5.13, we show the progress variable contours at different simulation times for the THAI HD-12 experiments. The flame propagation is faster along the axis of the facility than in other parts of the containment. This trend has also been observed in the experiments. The flame brush thickness is thin. This suggests that the turbulent eddies are not strong enough to penetrate the flame brush. That is, the flame is travelling in low turbulence region. The CFD simulation time for complete combustion is $t = 3.0s$.
The validation results for the Lipatnikov combustion model with THAI HD-12 experiments are shown in Fig. 5.14. Grid independence tests were performed and three levels of adaptive grid refinement are found sufficient to capture the flame propagation properties. The axial flame position as a function of time is shown in Fig. 5.14a. The flame moves too fast indicating that the flane velocity is over predicted. This can be seen in Fig. 5.14c showing the flame velocity as a function of time. The flame velocity profile is not well captured. In the CFD simulation, the initial flame acceleration is very high, resulting in the high flame velocity at the beginning of the flame propagation.

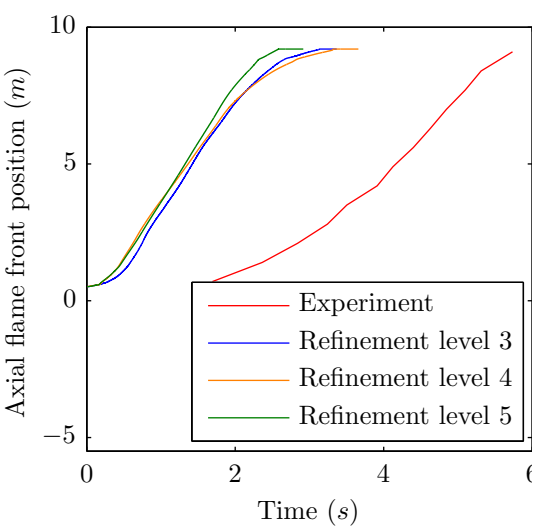

(a) Flame position

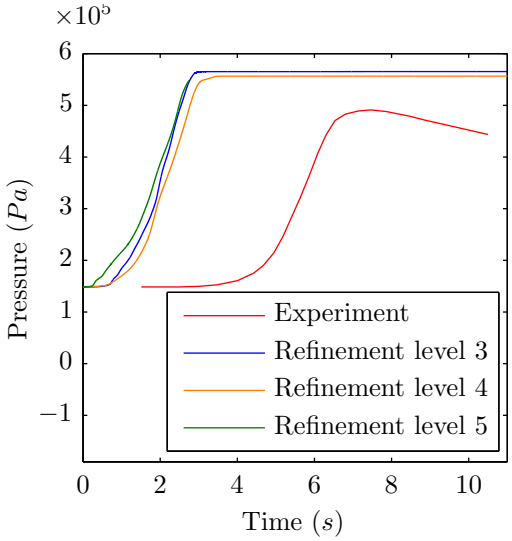

(b) Pressure development

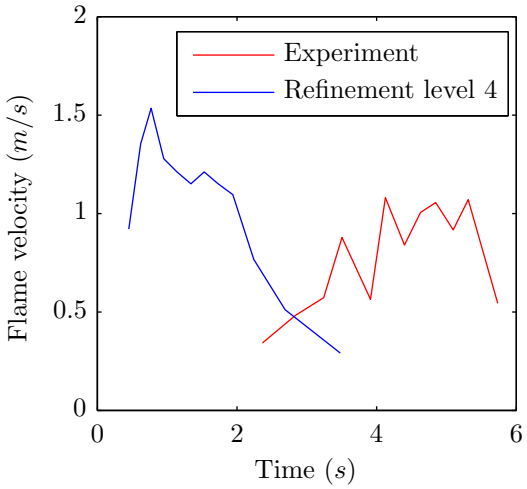

(c) Flame velocity

Figure 5.14: Validation results for THAI HD-12 experiment using Lipatnikov combustion model

The pressure development in THAI facility is shown in Fig. 5.14b. Strictly speaking, the grid independent results are not obtained for the pressure development. Increasing the adaptive grid refinement level increases the rate of pressure rise especially in the beginning of the burning process. However, the difference is very small and the slope of the pressure profile is practically similar in all the cases. In the CFD simulations, we can see a high pressure rise in the beginning of the combustion process. This indicates that the initial burning rate is over predicted in the beginning. However, the slope of pressure profile is qualitatively in good agreement with that of experiments. The end pressure is at the AICC value since no heat losses from the walls of test facility are considered.

Comparison Lipatnikov and Zimont model

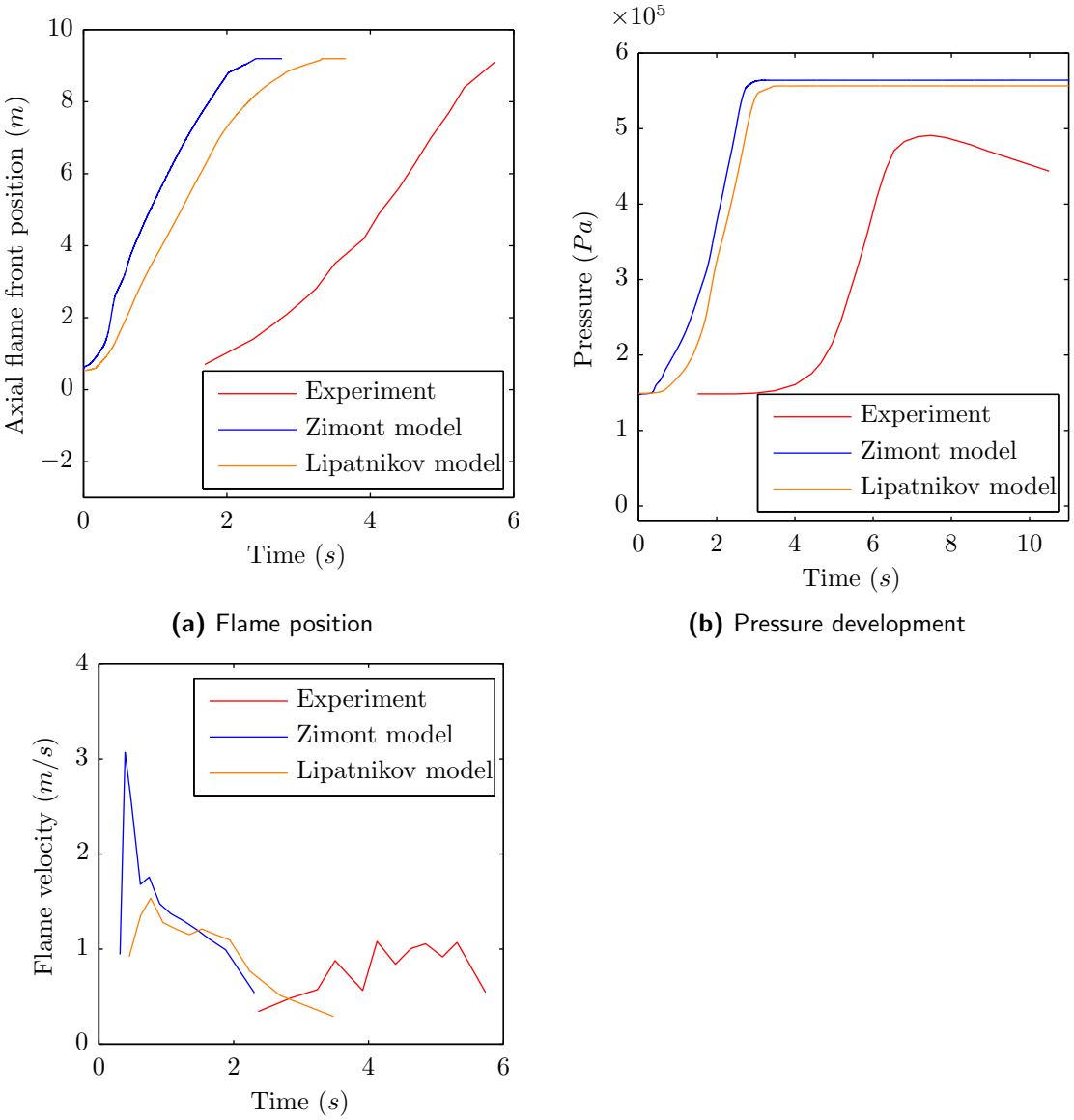

(a) Flame position

(b) Pressure development

(c) Flame velocity

Figure 5.15: THAI HD-12 experiment comparison for Zimont and Lipatnikov combustion model

In Fig. 5.15 we have compared the flame propagation in the Zimont and the Lipatnikov combustion model. We see that the Lipatnikov combustion model is the better performing combustion model in this facility. For the Lipatnikov combustion model, we see that: 1) the flame propagation is slow (see Fig. 5.15a), 2) the flame velocity is less over predcited (see Fig. 5.15c), and 3) the pressure development is relatively slow (see Fig. 5.15b). These effects are due to the additional transient laminar source term in the progress variable equation.

5.2.4 THAI Lipatnikov model with radiation effects

In the THAI HD-12 experiment the time taken for complete combustion in the experiments is $t = 7.5s$. In the ENACCEF RUN-153 experiment, the corresponding time is $t = 0.15s$. Therefore, the burning time is much longer in the THAI HD-12 experiment, and thus, the radiation heat losses can have a bigger effect on the flame propagation and pressure development in the THAI facility. Therefore, as a next step, CFD simulation with consideration of radiation heat loss was performed to see its effect on flame propagation in the THAI HD-12 experiment.

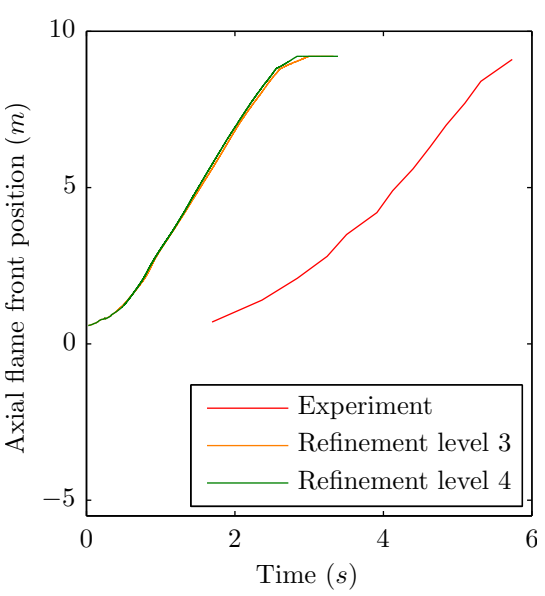

(a) Flame position

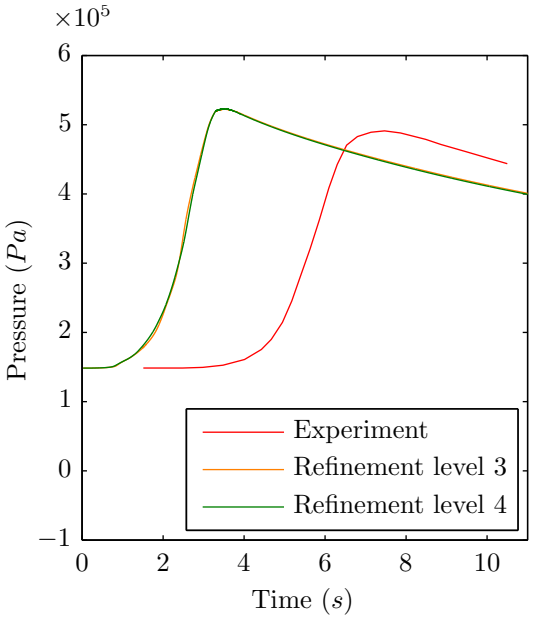

(b) Pressure development

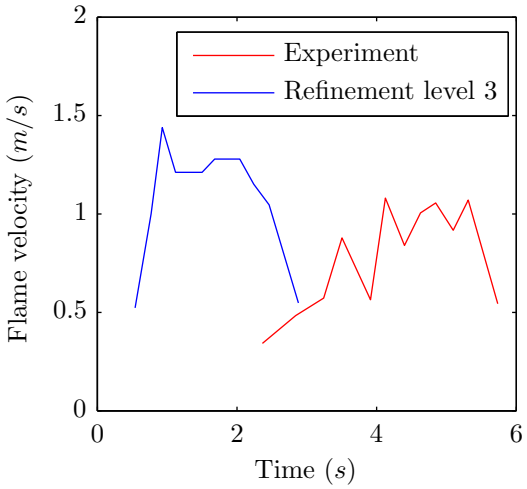

(c) Flame velocity

Figure 5.16: Validation analysis using THAI HD-12 experiment with Lipatnikov combustion model and DO thermal radiation model

The Lipatnikov combustion model is used to model the flame propagation and the DO

radiation model is used to model the thermal radiation heat losses. The absorption coefficient for the DO radiation model is determined by the in-house UDF for FLUENT developed by NRG. It is worth stressing here that this is the same UDF as used in the case of ENACCEF RUN-153 simulation in Section 5.1.3. The results for this simulation are presented in this section.

In Fig. 5.16, we show the validation analysis for the THAI HD-12 experiment using the Lipatnikov combustion model with the thermal radiation heat loss. Tests for adaptive grid independency were performed and three levels of adaptive grid refinement are found to be satisfactory to capture the flame propagation properties. In Fig. 5.16a, we see that, the flame is travelling too fast. The slope of the flame position is higher in the CFD simulations than in the experiment. This indicates that the flame velocity is over predicted, also shown in Fig. 5.16c. The reasons for this over prediction has been discussed frequently in the previous sections, but for the convenience of the reader these will be mentioned again. The reasons are: 1) presence of higher turbulence levels than what has been assumed or, 2) over prediction of turbulence levels by the $k - \epsilon$ turbulence model, or 3) over prediction of the source term in the progress variable equation.

In Fig. 5.16b, we can see the pressure development in the THAI HD-12 experiment. The slope of the pressure profile is qualitatively well predicted. Also, the decay in pressure following complete combustion is well captured by the DO radiation model. The slope of the pressure decay is in good agreement with the experiment. Thus, the radiation heat losses are indeed necessary to predict the decay in pressure after combustion.

Chapter 6

Conclusion

In this thesis work, we have have focussed on the flame propagation of uniform hydrogen-air mixtures in slow and fast deflagration regimes. Two combustion models have been considered: 1) the Zimont combustion model [4] and, 2) the Lipatnikov combustion model [5]. Furthermore, the effect and importance of thermal radiation on flame propagation is discussed. For the validation of combustion models, two different experiments in two different test facilities were chosen.

The first experiment, the ENACCEF RUN-153, is chosen to perform validation of fast deflagration flames. This facility has obstacles in the form of baffles which generate high turbulence, therefore the flame velocity is high in this experiment. The validation results for this case have been presented in Section 5.1. In Section 5.1.1, we have presented the Zimont combustion model results for ENACCEF RUN-153 experiment. The different flame propagation modes (quasi-laminar, acceleration, deceleration, and jet flame) have been successfully identified. Good qualitative and quantitative agreement has been obtained with the experiments. Section 5.1.2 presents the Lipatnikov combustion model results for the ENACCEF RUN-153. The different flame propagation modes have been successfully identified. Qualitative agreement with experiments is better than the Zimont combustion model (see Fig. 5.5). The time shift between the experiment and CFD simulation results is reduced. However, quantitatively the results are less well than the Zimont combustion model.
In Section 5.1.3, we have examined the effects of radiation heat loss in the ENACCEF RUN-153 experiment. The total combustion time in the experiment is very small $t = 0.15s$, and the effect of thermal radiation heat loss is not significant on flame propagation. The decay in pressure after complete combustion is well captured by the thermal radiation model. Thus, we observed that if the experimental burning time is very small then radiation heat loss does not affect the flame position or pressure development. However, it is necessary to perform validation analysis on few more experiments with small burning time to make a confident statement. But indeed thermal radiation heat losses does help in predicting the decay in pressure after the complete combustion of the unburned products.

The second experiment, the THAI HD-12 experiment, is performed for the validation of slow deflagration flames. This is a relatively simple vessel type geometry with no obstacles and the flame velocity remains low. The results for this case have been presented in Section 5.2. In Section 5.2.1, validation results using the Zimont combustion model are presented. Flame propagation is fast along the axis of the geometry, as is also observed in experiments. However, the flame propagation velocity is highly over predicted. In Section 5.2.2 we have presented the validation analysis using the Zimont combustion model but without including PDT instability effects. This has been done because other research groups such as that of Hoyes et al. [32] have presented the validation results using this method. However, it is has been discussed that this method is incompatible with the physical nature of the low concentration hydrogen-air flames, since such flames are born with PDT instabilites. It is stressed that, even though we have good results, the method is incorrect and should NOT be used. In Section 5.2.3 we have presented the HD-12 validation results using the Lipatnikov combustion model, and compared with those of the Zimont combustion model. Here we see that the flame velocity predicted by the Lipatnikov combustion model is much less than that of the Zimont combustion model. Consequently, the flame position from the Lipatnikov combustion model is in more agreement with the experimental results. However, the flame velocity is still over predicted with respect to the THAI HD-12 experiment. It has been stressed frequently in this report that the reason for over prediction of flame velocity could be 1) the presence of higher turbulence levels than assumed by us, or 2) the high turbulence levels predicted by the $k-\epsilon$ turbulence model, or 3) the over prediction of source term by the combustion model in the progress variable equation. It has been observed that the complete combustion time in the THAI HD-12 experiment $t = 7.5s$ is considerably longer and the flame speed and pressure development is affected by the radiation heat loss. This effect has been shown in Section 5.2.4, and the results with thermal radiation heat loss agree more with the experimental results. Thus, we see that the effect thermal radiation is significant for longer burning times.

Finally, we observe that the Lipatnikov combustion model gives qualitative better results, and is thus a melioration over the Zimont combustion model. Furthermore, the effects of thermal radiation heat losses are necessary as they can affect the flame propagation and pressure development. Thus, Lipatnikov combustion model combined with thermal radiation heat loss should further be used for investigation purposes.

Chapter 7

Recommendations for future work

In this thesis work we have presented the validation analysis for two experiments with slow and fast deflagrations. In the author's opinion, the validation results for the THAI slow deflagration tests need more attention. As an immediate next step validation analysis should be performed for the other experiments performed in the THAI facility (see Fig. B.1), and compare if the same trend in the experiments and the CFD simulations can be observed(see Sec. B.4 for post processed experimental data). We are using the $k-\epsilon$ turbulence model, which does not takes into account the wall effects and over predicts the turbulence. Thus, a study on the effects of turbulence model should be performed. In the THAI HD-12 simulation we have used a 2-D geometry and assumed axisymmetric flame propagation. This has been done to save the computational costs involved. But as a next step the simulations for 3-D geometry should be performed.

We have performed the validation in the ENACCEF test facility which is $5m$ high, and in the the THAI test facility which is $9.2m$ high. The author suggests that validation studies should also be performed in bigger facilities such as FLAME test facility $30m$ [33] and RUT test facility $65m$ [34].

It is worth mention that we have performed validation study for uniform hydrogen-air mixtures. However, in case of a real accident, this will not be the case and the hydrogen concentration could be non-homogeneous. Thus, validation with non-homogeneous hydrogen-air mixtures is also imperative. Also, in case of an accident, it is possible that we have hydrogen-air-steam mixtures. Therefore, validation study of these mixtures with varying concentration of steam and hydrogen should also be performed.

With this work the author has made an attempt to create a base for further validation studies of Lipatnikov combustion model and hopes that this study will stimulate interest to further improve this combustion model.

References

[1] M.P. Sherman. Hydrogen combustion in nuclear plant accidents and associated containment loads. *Nuclear Engineering and Design*, 82(1):13 – 24, 1984.

[2] Three mile island. *Technology and Society*, 7(28):9–11, 1979.

[3] Takashi Tsuruda. Nuclear power plant explosions at fukushima-daiichi. *Procedia Engineering*, 62(0):71 – 77, 2013. 9th Asia-Oceania Symposium on Fire Science and Technology.

[4] V.L. Zimont. Gas premixed combustion at high turbulence. turbulent flame closure combustion model. *Experimental Thermal and Fluid Science*, 21(13):179 – 186, 2000.

[5] A.N. Lipatnikov and J. Chomiak. Turbulent flame speed and thickness: phenomenology, evaluation, and application in multi-dimensional simulations. *Progress in Energy and Combustion Science*, 28(1):1 – 74, 2002.

[6] Thierry Poinsot and Denis Veynante. *Theoretical and Numerical Combustion*. R. T. Edwards, Inc., 2001.

[7] G. Ciccarelli and S. Dorofeev. Flame acceleration and transition to detonation in ducts. *Progress in Energy and Combustion Science*, 34(4):499 – 550, 2008.

[8] Pratap Sathiah, Steven van Haren, Ed Komen, and Dirk Roekaerts. The role of cfd combustion modeling in hydrogen safety managementii : Validation based on homogeneous hydrogenair experiments. *Nuclear Engineering and Design*, 252(0):289 – 302, 2012.

[9] James F. Driscoll. Turbulent premixed combustion: Flamelet structure and its effect on turbulent burning velocities. *Progress in Energy and Combustion Science*, 34(1):91 – 134, 2008.

[10] Fushui Liu, Xiuchao Bao, Jiayi Gu, and Rui Chen. Onset of cellular instabilities in spherically propagating hydrogen-air premixed laminar flames. *International Journal of Hydrogen Energy*, 37(15):11458 – 11465, 2012.

[11] A.N. Lipatnikov and J. Chomiak. Molecular transport effects on turbulent flame propagation and structure. *Progress in Energy and Combustion Science*, 31(1):1 – 73, 2005.

[12] N. Peters. Laminar flamelet concepts in turbulent combustion. *Symposium (International) on Combustion*, 21(1):1231 – 1250, 1988.

[13] N. CHAUMEIX and A. BENTAIB. Sarnet h2 combustion bnechmark. Technical report, Bureau de Physique des Accidents Graves, IRSN, 2010.

[14] T. Kanzleiter and G. Langer. Hydrogen deflagration tests hd-2r and hd-12. Technical report, Becker Technologies GmbH, 2008.

[15] Verbecke Franck. *Formation and Combustion of Non-Uniform Hydrogen-Air mixtures*. PhD thesis, University of Ulster, 2009.

[16] Nilanjan Chakraborty and Stewart Cant. Unsteady effects of strain rate and curvature on turbulent premixed flames in an inflowoutflow configuration. *Combustion and Flame*, 137(12):129 – 147, 2004.

[17] Denis Veynante and Luc Vervisch. Turbulent combustion modeling. *Progress in Energy and Combustion Science*, 28(3):193 – 266, 2002.

[18] B.Scott Brewster, Steven M. Cannon, James R. Farmer, and Fanli Meng. Modeling of lean premixed combustion in stationary gas turbines. *Progress in Energy and Combustion Science*, 25(4):353 – 385, 1999.

[19] U. Bielert, A. Kotchourko, B. Burgeth, and W. Breitung. Numerical simulation of large scale hydrogen explosions in complex geometries. *ZAMM - Journal of Applied Mathematics and Mechanics / Zeitschrift fr Angewandte Mathematik und Mechanik*, 81(S3):519–520, 2001.

[20] M Manninen, A Silde, I Lindholm, R Huhtanen, and H Sjvall. Simulation of hydrogen deflagration and detonation in a {BWR} reactor building. *Nuclear Engineering and Design*, 211(1):27 – 50, 2002.

[21] D. Baraldi, A. Kotchourko, A. Lelyakin, J. Yanez, P. Middha, O.R. Hansen, A. Gavrikov, A. Efimenko, F. Verbecke, D. Makarov, and V. Molkov. An intercomparison exercise on {CFD} model capabilities to simulate hydrogen deflagrations in a tunnel. *International Journal of Hydrogen Energy*, 34(18):7862 – 7872, 2009.

[22] D. Baraldi, A.G. Venetsanos, E. Papanikolaou, M. Heitsch, and V. Dallas. Numerical analysis of release, dispersion and combustion of liquid hydrogen in a mock-up hydrogen refuelling station. *Journal of Loss Prevention in the Process Industries*, 22(3):303 – 315, 2009.

[23] H. Wilkening and D. Baraldi. {CFD} modelling of accidental hydrogen release from pipelines. *International Journal of Hydrogen Energy*, 32(13):2206 – 2215, 2007.

[24] D. Makarov, F. Verbecke, V. Molkov, A. Kotchourko, A. Lelyakin, J. Yanez, D. Baraldi, M. Heitsch, A. Efimenko, and A. Gavrikov. An intercomparison of {CFD} models to predict lean and non-uniform hydrogen mixture explosions. *International Journal of Hydrogen Energy*, 35(11):5754 – 5762, 2010.

[25] Vladimir Molkov, Dmitriy Makarov, and Jonathan Puttock. The nature and large eddy simulation of coherent deflagrations in a vented enclosure-atmosphere system. *Journal of Loss Prevention in the Process Industries*, 19(23):121 – 129, 2006.

[26] V.V. Molkov, D.V. Makarov, and H. Schneider. Hydrogen-air deflagrations in open atmosphere: Large eddy simulation analysis of experimental data. *International Journal of Hydrogen Energy*, 32(13):2198 – 2205, 2007.

[27] V. Molkov, F. Verbecke, and D. Makarov. Les of hydrogen-air deflagrations in a 78.5-m tunnel. *Combustion Science and Technology*, 180(5):796–808, 2008.

[28] D. Makarov, F. Verbecke, V. Molkov, O. Roe, M. Skotenne, A. Kotchourko, A. Lelyakin, J. Yanez, O. Hansen, P. Middha, S. Ledin, D. Baraldi, M. Heitsch, A. Efimenko, and A. Gavrikov. An inter-comparison exercise on {CFD} model capabilities to predict a hydrogen explosion in a simulated vehicle refuelling environment. *International Journal of Hydrogen Energy*, 34(6):2800 – 2814, 2009.

[29] D. Baraldi, A. Kotchourko, A. Lelyakin, J. Yanez, A. Gavrikov, A. Efimenko, F. Verbecke, D. Makarov, V. Molkov, and A. Teodorczyk. An inter-comparison exercise on {CFD} model capabilities to simulate hydrogen deflagrations with pressure relief vents. *International Journal of Hydrogen Energy*, 35(22):12381 – 12390, 2010.

[30] Pratap Sathiah, Ed Komen, and Dirk Roekaerts. The role of cfd combustion modeling in hydrogen safety management-part i: Validation based on small scale experiments. *Nuclear Engineering and Design*, 248(0):93 – 107, 2012.

[31] S. R. Gubba, S. S. Ibrahim, W. Malalasekera, and A. R. Masri. An assessment of large eddy simulations of premixed flames propagating past repeated obstacles. *Combustion Theory and Modelling*, 13(3):513–540, 2009.

[32] J. R. Hoyes1, H. S. Ledin, and A. A. K. Tehrani. Benchmarking on hydrogen deflagrations isp - 49: Cfd modelling capabilities and limitations. volume NURETH15-271, 2012.

[33] M.P. Sherman, S.R. Tieszen, and W.B. Benedick. The effect of obstacles and transverse venting on flame acceleration and transition to detonation for hydrogen-air mixtures at large scales. Technical report, U.S. Nuclear Regulatory Commission, 1989.

[34] W. Breitung, S. Dorofeev, A. Kotchourko, R. Redlinger, W. Scholtyssek, A. Bentaib, J.-P. LHeriteau, P. Pailhories, J. Eyink, M. Movahed, K.-G. Petzold, M. Heitsch, V. Alekseev, A. Denkevits, M. Kuznetsov, A. Efimenko, M.V. Okun, T. Huld, and D. Baraldi. Integral large scale experiments on hydrogen combustion for severe accident code validation-hycom. *Nuclear Engineering and Design*, 235(24):253 – 270, 2005.

Appendix A

ENACCEF experiment

A.1 List of experiments

Table A.1: Experiments performed in ENACCEF facility

Experiment	Hydrogen concentration	Blockage Ratio	Mixture %
765	11.6-8.1	0.63	5.13%
736	11.4-5.8	0.63	6.24%
733	5.7-12	0.63	-16%
160	13	0	-67.5%
158	13	0.33	2.34%
153	13	0.63	-6.11%

A.2 Zimont combustion model

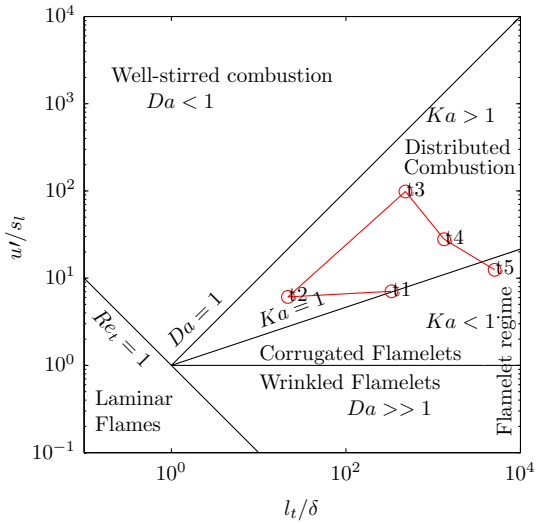

Figure A.1: Borghi diagram for ENACCEF RUN-153 using Zimont combustion model

A.3 Lipatnikov combustion model

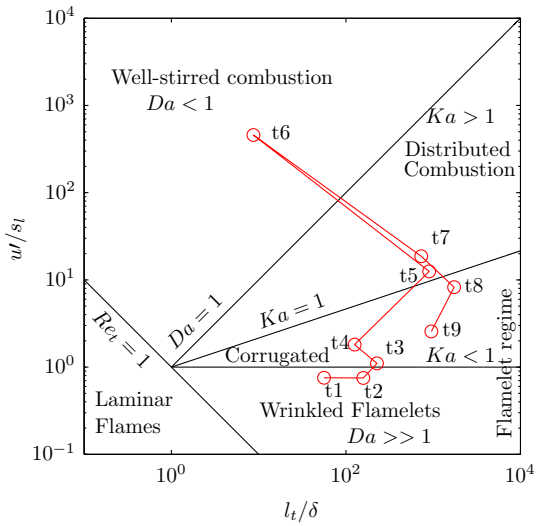

Figure A.2: Borghi diagram for ENACCEF RUN-153 using Lipatnikov combustion model

Appendix B

THAI-HD experiment

B.1 THAI Hydrogen Deflagration experiments

Test no.*)	Test date	P_0 bar	T_0 °C	C_{H2} vol%	C_{steam}	Burn direction	Pmax bar	T_{max} °C
HD-1R	06/12/2007	1.493	25	6.1	0	up	2.9	330
HD-2R	04/12/2007	1.492	18	8.1	0	up	5.05	765
HD-3	05/12/2007	1.485	22.5	9.0	0	up	5.6	850
HD-4	07/12/2007	0.996	24	6.0	0	up	1.98	350
HD-5	10/12/2007	1.170	20.5	7.5	0	up	3.4	665
HD-6	13/12/2007	1.485	19.5	7.0	0	up	3.65	495
HD-7	18/12/2007	1.480	17	9.9	0	up	5.85	935
HD-8	19/12/2007	1.487	21.5	9.9	0	down	5.6	870
HD-9	20/12/2007	1.484	25	11.0	0	down	6.2	980
HD-10	20/12/2007	1.498	30	11.8	0	down	6.15	1040
HD-11	21/12/2007	1.495	27	8.9	0	down	5.35	825
HD-12	15/01/2008	1.485	18	8.0	0	up	4.92	750
HD-13	17/01/2008	1.476	20.5	8.2	0	down †	4.65	720
HD-14	18/01/2008	1.510	28	8.7	0	down	4.2	680
HD-15	24/01/2008	1.504	93	9.9	0	up	4.95	950
HD-16	25/01/2008	1.492	92	12.0	0	down	5.5	1080
HD-17	29/01/2008	1.505	135	10.0	0	up	4.55	965
HD-18	29/01/2008	1.498	136	9.9	0	down	4.35	935
HD-19	30/01/2008	1.493	137	12.0	0	down	5.1	1085
HD-20	30/01/2008	1.493	138	6.0	0	up	3.2	650
HD-21	31/01/2008	1.506	138	9.0	0	down	3.95	865
HD-22**	13/02/2008	1.487	92	9.9	25	up	**	**
HD-23**	14/02/2008	1.465	91	12.0	25	down	**	**
HD-24	15/02/2008	1.472	90.5	9.8	48	up	4.2	880
HD-25	18/02/2008	1.490	90 / 34	12.3 / 9.8	47 / 4	down	5.3	945
HD-26	19/02/2008	1.500	90 / 33	10.1 / 10.0	47 / 3	up	4.6	805
HD-27	20/02/2008	1.497	90 / 32	11.9 / 6.3	47 / 3	up	4	890
HD-28	21/02/2008	1.491	90.5 / 35	6.0 / 11.8	48 / 4	up	3.6	865
HD-29	22/02/2008	1.493	90.5 / 34	12.1 / 5.8	48 / 3.5	down	3.3	850
			(top / bottom)	(top / bottom)	(top / bottom)			

*) bold numbers = according to contracted test matrix (as updated in 2nd PRG meeting, Paris, 26/27 November 2007)
**) test proposed for blind post-test calculations
†) ignition only after initiation of fan

Figure B.1: THAI HD experiments

B.2 Temperature contours in THAI HD-12 experiment

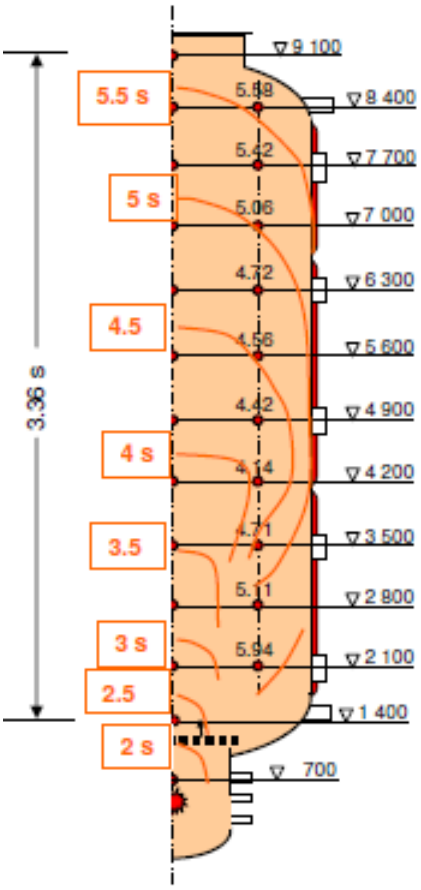

Figure B.2: Temperature profile from flame THAI HD-12 experiment

B.3 Base grid 8000 independency

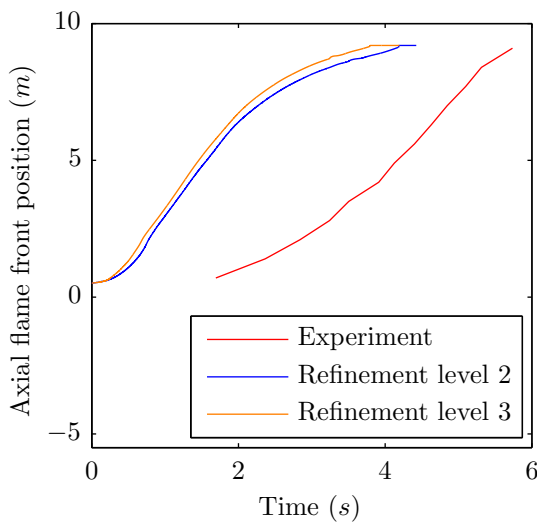

(a) Flame position, Base grid = 8000 cells

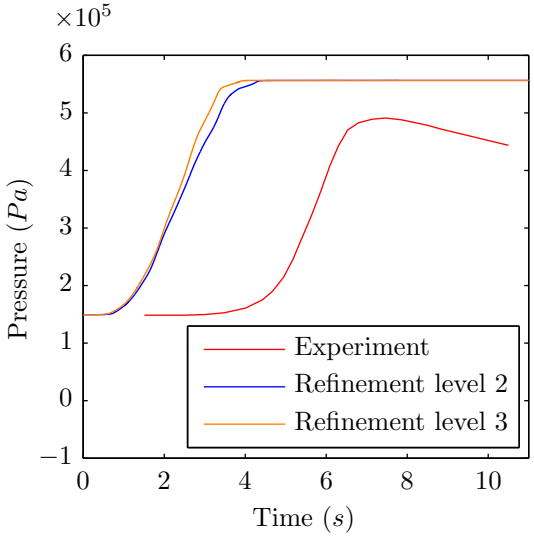

(b) Pressure development, Base grid = 8000 cells

Comparison of Lipatnikov model for base grid 2000 & 8000 cells

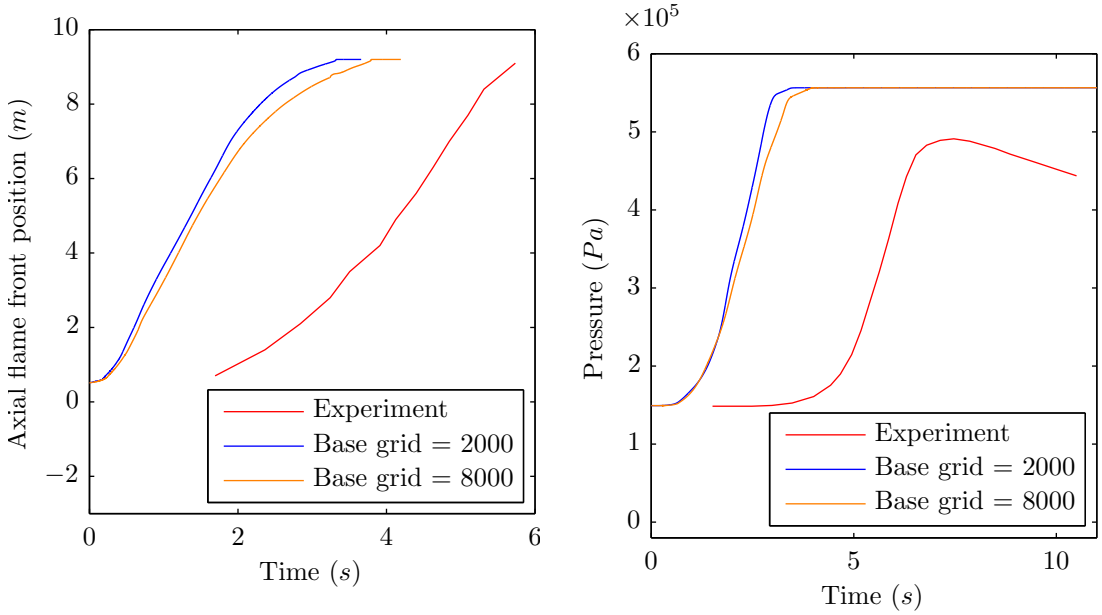

(c) Flame position **(d)** Pressure development

Figure B.3: Comparison for Base grid 2000 & 8000 in Lipatnikov combustion model

B.4 Experiments post processed data

B.4.1 Upward flame propagation

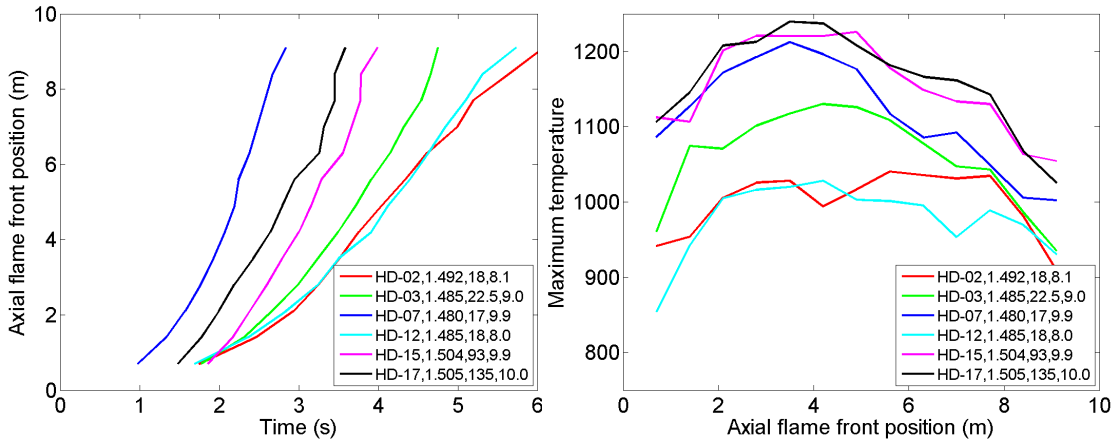

(a) Flame position **(b)** Maximum temperature at varying height

Figure B.4: THAI HD-experiments comparison for upward propagating flame

B.4.2 Downward flame propagation

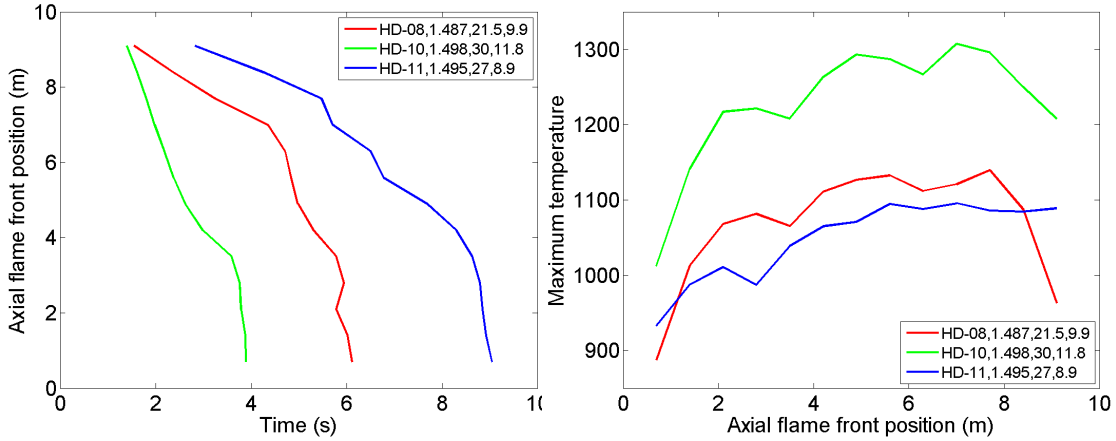

(a) Flame position **(b)** Maximum temperature at varying height

Figure B.5: THAI HD-experiments comparison for downward propagating flame